Imaging of the Canine Heart Using Non ECG-Gated 16 and ECG-Gated 64 Multidetector Row Computed Tomography

Diane C. Saulnier

Thesis submitted to the faculty of the Virginia Polytechnic Institute and State University in partial fulfillment of the requirements for the degree of

Master of Science
In
Biomedical and Veterinary Sciences

Reid Tyson
Gregory B. Daniel
Carolina Ricco

July 11, 2012
Blacksburg, VA

Keywords: canine, cardiac, computed tomography, MDCT

Imaging of the Canine Heart Using Non ECG-Gated 16 and ECG-Gated 64 Multidetector Row Computed Tomography

Diane C. Saulnier

ABSTRACT

ECG-gated multidetector computed tomography (MDCT) is an imaging modality widely utilized for the evaluation of cardiac pathology by physicians. However, there has been little research of cardiac MDCT imaging in veterinary patients. Presently, ECG-gating is an upgrade for MDCT, which few veterinary institutions currently possess. The purpose of this study was to compare image quality between a 16 non ECG-gated and 64 ECG-gated MDCT for clinically important cardiac anatomy in dogs. In a crossover trial, six dogs were scanned using 16 non ECG-gated and 64 ECG-gated MDCT. A standardized anesthetic protocol, designed to induce bradycardia (mean HR 45 bpm ± 12.6) was used. Five post-contrast sequential scans through the heart were performed for each patient when utilizing the 16 non ECG-gated MDCT, in attempt to obtain a motion free series of images of the heart. For each scan, assessment of cardiac morphology was performed by evaluating a group of 21 cardiac structures, using a 3-point scale. Each of the images were scored as 0 (motion present, scan non-diagnostic), 1 (motion present, scan diagnostic), and 2 (no motion, therefore diagnostic scan of high quality). Quality scores (QS) from all scans within a dog (30 scans total) were assigned for each cardiac structure. QS from the six ECG-gated MDCT scans were of high diagnostic quality, generating diagnostic images for all of the 21 cardiac structures evaluated for each of the 6 scans. Individual non ECG-gated scans were of variable quality, primarily generating QS of 1 or 2. A complete set of diagnostic images for all 21 structures was not achieved from an individual scan. Minimum number of non ECG-gated scans to identify a single structure was calculated, and ranged from 1-2 scans for all structures. Cumulative number of sequential non ECG-gated scans needed to achieve images of all cardiac structures was

calculated and determined to be 5. A 16 non ECG-gated MDCT scanner can produce cardiac images that are similar in quality, to those of 64 ECG-gated MDCT. Cardiac motion negatively impacts image quality in studies acquired without ECG-gating. However, this can be overcome by performing multiple sequential scans through the heart.

Table of contents

Table of Figures

Chapter 1: Introduction

Since its conception, over a quarter of a century ago, the utilization of computed tomography by the medical community has grown exponentially. This is largely a result of the unique capabilities of this non-invasive imaging modality to generate images that allow visualization of structures of interest without superimposition of overlying anatomy. Technological advances, since its introduction in 1972, have resulted in short acquisition times and superior spatial and contrast resolution. Initial rudimentary single slice capability and study acquisitions that took over 9 hours to reconstruct, hampered widespread early adoption of the technology. Today, computed tomography scanners have been produced that are able to perform 320 slices at one, with gantry rotation times of less than 500ms. A significant milestone that augmented this evolution of CT technology was the development of the slip ring, first introduced in 1988. The slip ring design allowed for continuous rotation of the X-ray tube without the need for it to unwind the cords associated with the gantry. This pioneering technology was largely responsible for decreasing temporal resolution, enabling imaging of moving anatomy.

Computed tomography is an extremely versatile imaging modality that has been applied to imaging of all body systems, including the uniquely challenging cardiovascular system. A survey of CT imaging centers around the country indicated that over 70 million CT procedures are performed annually in the United States alone, with an annual increase in CT procedures approximating 19% from the years 1991-2002. [1] The number of cardiac CT procedures performed has had an annual growth rate of 145%. [2] Computed tomography has proven to be successful for the evaluation of the heart including both normal morphologic features and pathology of the cardiac

chambers, valves, coronary arteries and pulmonary veins. It has also been employed for functional imaging of the heart. [3] Although GE, Philips, Siemens and Toshiba dominate the computed tomography market as manufacturers, over 50 companies worldwide contribute to continued CT research and development.[4] Each of the four major manufacturers offer a 64 MDCT equipped with ECG gating. Although further advances in technology have been made that allow improved temporal and spatial resolution, at this time 64 MDCT is considered the gold standard for cardiac imaging and is quickly replacing its predecessor, fluoroscopic guided cardiac angiography. Unfortunately, the manufacturers, physicists, engineers, cardiologists, radiologists and researchers contributing to the evolution of this imaging modality have been unable to agree on standardized CT terminology. Consequently, the literature is confused with synonymous terms for the technology, concepts and CT procedures. The Society of Cardiovascular Computed Tomography released a guide for standardized medical terminology for cardiac computed tomography, which has been adhered to throughout the entirety of this paper.[5]

Although cardiac computed tomography has proven to be an effective diagnostic tool in the medical arena, it remained unutilized by the veterinary community until its introduction into the veterinary literature in 2011. At this time the modality was proven to be an effective diagnostic imaging procedure for the evaluation of the canine coronary arteries.[6] Over the last 3 decades, the use of cardiac computed tomography has become a mainstay for the diagnosis of cardiac disease in the human patient. However, it has largely been ignored as a diagnostic tool by the veterinary community. The goal of this study was to determine the feasibility of utilizing non ECG-gated 16 MDCT and ECG-gated 64 MDCT to produce diagnostic images of the normal canine cardiac

morphology. A secondary goal was to develop a general protocol that could be used as a guideline by the veterinary community for cardiac imaging.

Normal cardiac and great vessel anatomy

General Description

The heart is a specialized four-chambered muscular pump that simultaneously drives, in series, two separate circulation pathways of blood within the body.[7] The left side of the heart, which consists of the left atrium and ventricle, maintains forward flow of systemic circulation, while the right atrium and ventricle drive pulmonary circulation. Together, a fibrocartilage base, which serves as scaffolding, and the myocardium, form the walls of the four-chambered organ. This fibrocartilage base is composed of two fibrous rings (annuli fibrosi) that circumscribe the apertures of the atrioventricular orifices and two short annular conduits that form the base of the aortic and pulmonary trunks. Each of these four rings serves as attachment sites for internal valves.[8,9] In effect, the fibrocartilage skeleton, with its associated valves, serve to separate the atria, from the ventricles and also to prevent backflow of pulmonary or systemic blood into the heart. Orientation of the heart within the thoracic cavity is influenced by breed and the presence of pathology. However, generally speaking, the long axis of the canine heart is typically positioned in a craniodorsal to caudoventral orientation that describes a 45 degree angle to a dorsal plane through the thorax. The apex of the heart is positioned to the left of midline, resting in a caudoventral and left lateral position. It is positioned within the mediastinum. [8]

The chambers and great vessels of the heart have a complex anatomic relationship. The craniodorsal surface of the heart, which is also the widest region of the organ, is designated the base of the heart. This surface is where the great vessels enter and exit the organ. From dorsal, the right and left atria are positioned along the cranial and left lateral margins of the base of the heart, respectively. This region of the heart has been deemed, the "auricular surface". The pulmonary trunk is juxtaposed between these two atrial structures as it projects from its origin of the conus arteriousus of the right ventricle. Along the right lateral and caudal margins of the heart base is the right and left atrial surfaces, respectively. The right and left atria are positioned along the right lateral and caudal margins of the base, positioned dorsal to their ventricular counterparts. [8,9]

Heart wall and pericardium

The myocardium is subdivided into the contracting myocardium, which is the primary component of the heart wall, and the stimulus conducting myocardium. The thickness of the myocardium varies within the four chambers of the normal heart, and is a direct reflection the pressure differences experienced by the atria and ventricles. The myocardium consists of striated cardiac muscle cells that are arranged in three layers, the external, middle and internal. The heart chambers are lined with a thin endothelial layer, called the endocardium. This layer of thin tissue also covers the heart valves and is contiguous with the lining of the great vessels as they make their entrance or exit from the heart chambers. The surface of the heart is encased in a thin layer of mesothelial cells, the epicardium. At the heart base, the visceral epicardial layer reflects back and continues as the thin serous lining, or parietal pericardium, that is adherent to

the fibrous outer pericardial layer that envelops the heart. At the heart base, the parietal and fibrous layers of the pericardium reflect onto the great vessels.[8]

Cardiac Chambers

Atria

The right (atrium dextrum) and left (atrium sinistrum) atrial chambers accommodate low-pressure blood flow that is received by the systemic and pulmonary circulatory systems, respectively.

Right atrium

The right atrium has a main part, the sinus venarum cavarum, which is positioned along the craniodorsal aspect of the base of the heart and is the recipient of the venous systemic blood. A smaller blind pouch, the right auricle or auricula dextra, projects off the cranial margin of the atrium. The right atrium receives the majority of the systemic venous blood flow from the cranial vena cava (vena cava cranialis), which empties into the chamber from a slightly craniodorsal direction and the caudal vena cava (vena cava cranialis), which enters from a caudodorsal direction. Blood from these vessels is directed through the aterioventricular valve by a semilunar ridge of muscle, the intervenous tubercle, that projects from the interatrial septum (septum interatriale). In some canine patients a small contribution of the systemic blood directly entering the right atrium is made from the azygous vein. However, this vessel typically is a tributary of the cranial vena cava, entering this larger vessel before it enters the right atrium. The right atrium also receives blood from the coronary sinus (sinus coronarius), which is a conduit for venous flow from the heart, the major contributor being the great

coronary vein. The coronary sinus is located along the left wall of the right atrium, ventral to the entrance of the caudal vena cava. Blood exits the right atrium through the right atrioventricular orifice (ostium atrioventriculare dextrum), passing into the right ventricle. Attached to the inner surface of the fibrous ring that constitutes the right atrioventricular orifice is the right atrioventricular valve (valva atrioventricularis dextra), also known as the tricuspid valve. [8]

Right ventricle

The right ventricle (ventriculus dexter) extends along the right lateral, right cranial and left cranial surfaces of the heart, conforming itself to the cone shaped left ventricle that resides along the caudodorsal aspect of the heart. In cross-section the lumen of the right ventricle is crescent shaped and the interventricular septum, which is the division between the two ventricles, is convex in shape. The myocardial free wall of the right ventricle is approximately 1/3 the thickness of the left ventricle, a direct reflection of the lower systolic pressure that it accommodates.[7] Internally, the luminal surface is characterized by myocardial ridges, called trabecula carneae. A muscular band, carrying conduction system fibers, extends from the interventricular septum to the ventricular free wall, traversing the right ventricular lumen. Systemic blood enters the ventricle through the right atrioventricular ostium and atrioventricular valve. The blood is then directed into a craniodorsal expansion of the right ventricle, the conus arteriosis by a muscular ridge of tissue, the supraventricular crest, that is positioned obliquely between the atrioventricular opening and the conus arteriosis. Blood leaves the right atrium through the pulmonary ostium with its associated pulmonary valve, the portal for blood to pass into the pulmonary trunk.

Left atrium

The left atrium (atrium sinistrum) is located along the caudodorsal aspect of the base of the heart. Similar to the right atrium, it has a main chamber off of which a small blind pouch, the left auricle (auricula sinistra), projects from. The left auricle projects from the left lateral aspect of the atrium. A variable number of pulmonary veins (typically 5-6) enter the left atrium. Typically pulmonary veins of the right lung pass dorsally to the right atrium to enter the craniodorsal aspect of the left atrium, while those from the left lung usually empty into its caudodorsal region. The pulmonary veins pass through openings into the chamber termed, pulmonary ostia (ostia venarum pulmonalium). [8,9]

Left ventricle

The left ventricle (venticulus sinister) is characterized by its conical shape and its thick muscular wall that tapers to form the apex of the heart. It is in a ventral location, relative to the left atrium. The left ventricle has a thick free wall with two large papillary muscles (musculi papillares) that project from its surface. As blood enters the left ventricular lumen it passes through the left atrioventricular orifice (ostium atrioventriculare sinistrum) and left atrioventricular valve. It is then directed in a craniodorsal direction, toward the base of the heart and propelled through the aorta. Blood from the left ventricle passes through the aorta, supplying the heart and rest of the body with oxygenated blood. [8,9]

Great vessels

Aorta

The aorta is separated from the left ventricle by the right, left and septal cusps of the aortic semilunar valve. Just distal to the aortic valve, the diameter of the ascending aorta focally increases, creating a bulbous region, the sinus of valsalva or the ortic bulb (bulbus aortae). Beyond the aortic bulb is a short ascending aorta, then the aortic arch, which continues dorsally and caudally as the descending aorta, which supplies systemic blood to the body.[8]

Coronary arteries

Originating from the walls of the aortic bulb, are sinuses (sinus aortae) that correspond to each of the three semilunar cusps of the valve, similarly designated the right, left and dorsal. The right and left sinuses house the orifices of the coronary arteries that supply the heart with oxygenated blood. As the coronary arteries leave their respective sinuses, the travel across the surface of the heart within grooves that roughly mimic the internal divisions within the heart. There are 3 grooves that traverse the surface of the heart; the coronary groove, the subsinuosal interventricular groove and the paraconal interventricular groove. The coronary groove (sulcus coronarius), encircles the base of the heart, for the exception of the cranioventral region, where the conus arteriousus of the right ventricle crosses dorsally and to the left of midline, preventing completion of the coronary grooves circuitous route. The coronary groove, and the left circumflex artery that travels within it, marks the separation between the atria and ventricles. The subsinuosal interventricular groove (sulcus interventricularis subsinuous) is located along the caudal margin of the heart, extending from the ventral aspect of the caudal vena cava, ventrally toward the apex, demarcating the position of the interventricular septum. Finally, the paraconal interventricular

groove originates from under the left auricle, travelling along the left lateral side of the heart, traveling cranioventrally ending before the apex. This groove roughly parallels the cranial margin of the right ventricle with the left ventricle. Within it travels the paraconal interventricular branch of the left coronary artery. [8,9]

Right coronary artery

The right coronary artery (a. coronaria dextra) is typically slightly smaller in diameter than the left coronary artery. After leaving the right sinus, it takes a semicircular route to the right, passing over the surface of the conus arteriosus of the right ventricle, becoming caudodorsal in its path as it passes ventral to the right auricle on its way to the caudodorsal most aspect of the right ventricle. Along its course over the right ventricle, smaller vessels originate from it, extending over the surface of the chamber. In 20% of dogs, an accessory right coronary artery, arises from the right sinus, adjacent to the main coronary artery. It travels cranioventrally along the conus arteriosus, where it terminates after a short course.[10] The major contributor of oxygenated blood supplied to the right ventricle is via the right coronary artery. It also makes lesser contributions to the right atrium, ascending aorta and pulmonary trunk.

Left coronary artery

The left coronary artery (a. coronaria sinistra) originates from the left sinus as a solitary vessel that shortly thereafter bifurcates into two vessels, the circumflex and paraconal interventricular arteries. The latter of which is also termed the left cranial descending artery. The circumflex branch (ramus circumflexus) travels in a semicircular path within the coronary groove. As it branches from its origin, it travels in a

caudodorsal direction, passing ventral to the left auricle and continuing on to partially encircle the left atrium. As it reaches its caudal most extent, it turns ventrally, coursing toward the cardiac apex as the subsinuosal interventricular branch (ramus interventricularis subsinuosus) in the subsinuosal interventricular groove. The subsinuosal interventricular branch has a variable termination, ending proximal to, at or past the apex of the heart. This groove marks the approximate location of the interventricular septum. The circumflex artery has a variable number of ventricular branches ranging from 4–11.[8] It supplies the left atrium, left auricle and a portion of the interventricular septum.[8] The subsinuosal interventricular branch supplies the left ventricle and portions of both the right ventricle and interventricular septum. The second artery to bifurcate from the origin of the left coronary artery is the paraconal interventricular artery, also known as the cranial descending artery. After branching from the left coronary artery, it travels ventrally and slightly caudally in an oblique direction. Its distal most extent winds cranially from left to right, around the apex, ending on the right side of the heart, ventral to the right ventricle. It takes this course while travelling in the paraconal interventricular groove. The septal branch, which has a variable origination, originates from the paraconal interventricular branch, terminal branch of the left coronary artery, left coronary artery, aorta or circumflex branch, listed in descending order of frequency.[8] The septal branch is the primary provider of oxygenated blood for the interventricular septum. [8,9]

Pulmonary vessels

The pulmonary artery is an outflow tract that provides a route of passage for unoxygenated blood to exit to the lungs. It originates from the conus arteriousus of the

right ventricle. Given that the conus arteriosus is positioned in a cranioventral and right lateral to craniodorsal and left lateral orientation, the main pulmonary artery exits the heart cranially and to the left of midline. It then bifurcates into the right and left pulmonary arteries. Given their position to the left of midline, the right pulmonary artery must cross to the right before it can supply the right lung. At the base of the pulmonary artery is the pulmonic valve, which consists of right, left and intermediate semilunar cusps.[8,9]

Coronary cardiac anomalies

Historically, diagnosis of canine congenital cardiac anomalies has been dependent on angiocardiography and echocardiography. However, given the cross-sectional nature of computed tomography, where images can be generated without superimposition of overlying structures, CT has the potential to be an imaging modality that is more suitable for evaluation of cardiac morphology. Thus far it has been minimally utilized in the veterinary community for this purpose. Unlike human medicine, nearly all echocardiograms are performed by veterinarians, not trained sonographers. Echocardiography is technically demanding, particularly for the evaluation of complex congenital abnormalities. Since there are few trained veterinary cardiologists, computed tomography may represent an alternative method to evaluate complex congenital cardiac disease in animal patients, particularly when trained expertise is not readily available.

Computed tomography could be particularly useful in regard to the diagnosis of anomalous coronary arteries. A relationship between pulmonary stenosis, secondary to an anomalous right coronary artery in the English Bulldog, and to a lesser extent in the

Boxer, has been established in the veterinary literature.[11-15] In affected patients, a single right coronary artery gives rise to the origin of the left coronary artery, instead of originating from their prospective aortic sinuses. This proximal part of the left coronary artery then transcribes the pulmonary artery in its route to the left side of the heart. Given its circumscribed route around the pulmonary trunk, this particular type of anomalous coronary artery distribution, termed R2A, causes constriction of the right ventricular outflow tract at the level of the pulmonary valve, resulting in pulmonic stenosis.[11,12] Three additional anomalous right coronary distributions have been described. However, the course of the left coronary artery is not circumpulmonary in its route in these other described anomalies.[11]

Correct diagnosis of the R2A coronary artery anomaly is of particular significance, because of its association with pulmonic stenosis and the method of treatment for this disease. Pulmonic stenosis can be corrected through balloon-dilation valvuloplasty, where the region of stenosis is expanded by distention of the balloon of a balloon valvuloplasty catheter.[16,17] A second approach for correction of pulmonic stenosis is through a direct surgical approach where a patch-graft procedure is utilized to make an incision in the region of stenosis where a piece of polytetrafluoroethylene can be sewn in, in effect increasing the size of the pulmonary outflow tract.[16] Without prior knowledge of a circumpulmonary artery, either of these procedures will likely result in disruption of the left coronary artery, leading to myocardial infarction and sudden death.[14,16]

Although transthoracic echocardiography may be the preliminary diagnostic test employed to evaluate cardiac disease, MDCT angiography and cardiac MR angiography (MRA) are widely utilized and well established in the human literature. Congenital

coronary anomalies within the general population are thought to be 1-2%.[18] The majority of these anomalies are of little clinical significance. However, approximately 20-30% of these congenital anomalies are of hemodynamic significance and can lead to sudden death if undiagnosed.[19,20] Sixty four slice MDCT with ECG gating is regarded as being an optimal modality for evaluation of the coronary arteries. Computed tomography is able to clearly demonstrate the origin of the coronary arteries from the aortic ostia to their termination, clearly defining any anomaly that may be present. Conventional angiography is becoming less frequently utilized because of it's invasive nature and because it is a two-dimensional modality limited by the vascular overlap that sometimes obscures clear visualization of the coronary artery vasculature.[18] In a study by Ou et al, non ECG gated 64 MDCT and transthoracic echocardiography were compared for the evaluation of pulmonary vein stenosis. They concluded that non-gated MDCT angiography was a sensitive and specific way to evaluate pulmonary vein stenosis in pediatric patients and should be used as a complement to transthoracic echocardiography where pulmonary vein stenosis is suspected, but cannot be confirmed.[21]

Introduction to Computed Tomography

Computed tomography utilizes sophisticated hardware and software that creates tomographic images through the process of data acquisition, image reconstruction and manipulation. These images are stored in a picture archiving and communications system (PACS) in a standardized file format called the digital imaging and communication in medicine (DICOM). This standardized file format allows the images to be viewed using software from vendors with DICOM compliant technology.[22]

Modern day computed tomography scanners have the ability to obtain volume data of the patient at isotropic resolution, allowing reconstruction of lossless images in any anatomic plane. Computed tomography allows visualization of internal structures without superimposition of overlying structures, which is a distinct advantage when compared to other 2-dimensional cardiac imaging modalities, such as traditional radiography, angiocardiography, and echocardiography. Workstations with sophisticated DICOM viewers allow users to manipulate the volume data in a number of ways, including the creation of 3 and 4-dimensional data sets.

The History and Evolution of Computed Tomography

In 1917 Johann Radon put forth theoretical mathematical models that described the reconstruction of three-dimensional images from an infinite number of two-dimensional views. These theories were instrumental to the development of computed tomography, but could not be realized until computer technology was developed. Based on Radon's mathematical principles and the initial work conducted by Allen Cormack in 1964, , Sir Godfrey Hounsfield developed the first laboratory CT scanner that was able to reconstruct attenuation coefficients into an actual image of a slice of the human brain. The apparatus he built consisted of an x-ray tube and a detector set up to scan a preserved section of human brain. Scan time for the prototype CT took 9 hours for a single slice. Reconstruction of the scan data into an image took 2.5 hours. Regardless of this temporal restriction, this technology initiated a medical evolution of computed tomography when the first image of the brain revealed distinction between gray and white matter.[23]

By 1972 Hounsfield had utilized these basic principles to design a clinical prototype that was installed for use on clinical patients at Atkinson Morley's Hospital in London. The clinical prototype CT scanner consisted of a stationary-anode X-ray tube, sodium iodide crystal coupled to a photomultiplier tube and two detectors, which allowed 2 slices to be acquired simultaneously. This CT scanner prototype acquired images by means of translate-rotate movement of the x-ray tube and detectors. A pencil-beam X-ray source was employed and moved around the patient. After acquiring a single ray, the X-ray source and detectors would rotate 1 degree, for a total of 180 attenuation profiles. Performing a study of a head on the clinical prototype CT took 4.5 minutes to acquire and 1.5 minutes for image reconstruction. This prototype also proved its worth when a large hypodense cyst was found in the brain of the first clinical patient, thus setting the stage for the future of computed tomography.[23]

Principles of Computed Tomography

Basic Design of the CT Unit

Modern computed tomography units that are being employed in clinical settings have a fairly similar basic design. A CT unit consists of many components that allow it to effectively acquire, process, display and store the raw data that is collected during image acquisition. The basic components of the CT unit include the gantry, patient table, computer system for image reconstruction and manipulation, operator console, viewing console and a high frequency X-ray generator. The gantry is the housing for the X-ray tube, collimators, detector array, associated electronics (channels) and drive

motor. Centrally, the gantry has an aperture that accommodates the patient table, allowing it to pass between the x-ray tube and detectors during patient scanning [23,24]

The evolution of CT technology has been remarkable over the past three decades, each successive generation of CT scanner providing faster imaging with progressively higher spatial resolution. Initial first and second generation CT scanners utilized the time consuming method of "step and shoot" axial acquisition to generate single image slices through the subject. This technology required the gantry to be stopped following every rotation and its direction reversed. This allowed the ribbon cable, which was shared by the x-ray tube and detectors, to be spooled out and retracted after each rotation. Not only was this method time consuming, due to the long interscan delay between each slice acquisition, images often suffered from misregistration artifact due to the potential movement of anatomic structures between acquisitions of slices. This was due to patient movement that was voluntary or secondary to respiration or cardiac contraction. [25]

The introduction of slip ring technology, in 1988, enabled continuous helical rotation of the gantry allowed for faster scan times.[26] Slip ring technology is used in third generation CT systems where a rotate/rotate geometry allows both the x-ray tube and detector array rotate to around the patient.[22,25] Most modern CT units utilize the third generation design. A decade after the advent of slip ring technology, the modality was further advanced by the release of multidetector computed tomography (MDCT). MDCT increases the volume of data acquired in the z-axis during a single rotation of the gantry, by increasing the number of detector rows present in the detector array in the z-direction.[26] These two advancements, opened the door for exploration of improved vascular imaging.

X-ray tube

The X-ray tube utilized by CT technology is similar in design to that of the conventional X-ray unit. However, because of the demand for continuous X-ray production required with computed tomography, the thermal demand placed on these X-ray tubes is much greater. The basic X-ray tube design consists of a vacuum tube with a cathode (filament) and anode (target) that is enclosed in a housing unit. Longer interscan times, inherent with first and second generation scanners, allowed utilization of a x-ray tube with a stationary anode. Heat dissipation from the x-ray tube occurred during the interscan delay, allowing the tube to cool. Early x-ray tubes had heat capacities of 1 to 3 million heat units. With the development of helical CT, demands on the X-ray tube were increased because of the need for continuous X-ray production, without an interscan delay. To accommodate this many components of the x-ray tube were redesigned to deal with increased target temperature and need for better heat storage and dissipation. To increase the heat capacity of the x-ray tube, rotating-anodes with larger anode discs, graphite backing, circulating-oil heat exchangers and integration of newer more heat resistant materials for the rotor bearings and metal envelope were implemented. These changes have substantially increased the heat capacity of X-ray tubes to 5-8 million heat units, better serving the demands placed on it.

Detector Array Design

Conventional single slice CT units utilize a single row in the z-axis that is composed of 500-900 individual solid-state detector elements. This single detector row

describes an arc in the transverse plane.[26] The scan field-of-view is the amount of the patient anatomy that is included in the X-ray projection. A scan field of view of 50cm is typically utilized for routine scanning for humans.[25] After passing through the patient, numerous differentially attenuated X-rays are intercepted by the detector elements within a detector row. The combined rays or measurement values acquired at the same angular position of the measurement system are called a projection. Typically 1000 projections are measured during each 360-degree rotation of the gantry. The x-ray attenuation of the object is measured by the individual detector elements.

Modern CT scanners use scintillating solid-state detector elements. This light is detected by the photodiode region of the detector element and is amplified and converted into a digital electrical signal. The resultant data is transmitted through a single channel to its data acquisition system that converts the analog signals to digital signals in preparation for reconstruction of the raw data into images. Modern scintillators are constructed of ceramic materials and have high conversion rate and capture efficiency for the photons that strike its surface.[27] Materials used for the detectors also have a short afterglow decay time allowing fast gantry rotation times without the risk of cross talk. Overtime, with the drive to decrease acquisition times and increase volume coverage, the design of the CT unit evolved. Manufacturers continue to increase the number of data channels and detector rows, perpetuating the progression from single slice CT units with a single detector array to multislice computed tomographic units with 4, 8, 16, 32, 64 and 256 detector arrays in the z-axis.[28] The maximum number of image slices that can be acquired at one time is dictated by the number of image channels the CT unit has, not the number of detector rows in the z-axis.

Collimation

A tube collimator, also known as a pre-patient collimator, consists of a set of blades constructed of a high anatomic number, such as tungsten or molybdenum. These are used to shape the X-ray beam in the z-axis before it reaches the patient. In conventional single slice CT, the tube collimators determine the overall slice thickness, which is predetermined by the slice width selected by the user. In single slice CT, the maximum slice thickness that can be acquired is the width of the detector. Multidetector computed tomography also utilizes a pre-patient collimator. Its function is to determine the geometry of the x-ray beam and its width at the isocenter of the gantry. [24] With the advent of multidetector computed tomography and the increased number of detectors in the z-axis, the x-ray beam geometry had to be altered from the conventional pencil and fan beam shape that was employed with single slice detectors to a cone beam geometry. This geometry provides larger coverage of the detectors by the x-ray beam, in effect increasing the overall efficiency of the x-ray tube. However, it comes at the cost of increased patient exposure. The largest determinant of slice thickness in MDCT is the detector width and the selected detector configuration.

Multidetector design configurations are divided into uniform detector and non-uniform detector arrays. Uniform detector arrays, also known as matrix arrays, have detectors that are of the same width in the z-axis, or slice thickness direction. In non-uniform, or adaptive array detector configurations, the detectors in the z-axis are of unequal widths.

Cardiac CT

Early CT scanners were ill equipped to image the heart due to its inherent physiologic motion and the high temporal resolution needed to acquire images without motion artifact. In order to acquire images of a moving structure, without motion artifact, the acquisition must be faster than the speed at which the structure is moving. The temporal resolution of cardiac imaging for conventional cardiac angiography is approximately 20ms.

This obstacle of poor initial temporal resolution of CT was initially addressed by improving mechanical aspects of the CT scanner and development of ECG gating software that allowed selected reconstruction of CT studies based on phase of cardiac cycle. In initial CT designs, the mechanism of the CT scanner that limited the temporal resolution was the time it took for the gantry to rotate 360 degrees. Recognizing the need to improve temporal resolution and decrease scan time, steps were taken to improve gantry rotation time, including the development of slip ring technology. However, even with slip ring technology, which allowed continuous rotation of the tube in the same direction, rotation times could only be decreased to a certain point. This limitation was secondary to the large mechanical stresses placed on the gantry as a result of the G forces reached during rotation due to its great weight.[23] The mechanical support for the X-ray tube, tube collimator and detectors must be rigorous enough to provide stability of these components during gantry rotation.[25]

Rotation times of modern CT scanners range from 330-500 ms.[24] However, this has recently been decreased even further to 270ms. Cardiac imaging requires a temporal resolution of 250ms to be able to acquire an image through the heart during diastole without evidence of blur from motion. Temporal resolution of 50 ms is required for

imaging human patients with heart rates up to 70bpm. However, as the heart rate increases, the temporal resolution needed to image the heart without motion artifact also increases up to 100 -150ms because the diastolic phase becomes shorter.[29,30] Even with the advent of slip ring technology, gantry rotation time did not decrease to less than 330-500ms.[24] Some CT scanners are equipped with software designed to allow reconstruction of the cross-sectional image with just 180 degrees rotation. The temporal resolution for these machines is approximately half of the gantry rotation speed (165-250ms). [24]

During its infancy, cardiac CT was performed without the luxury of ECG-gating technology. However, in this capacity, cardiac CT was fairly limited in its scope. Initial experimental attempts to utilize computed tomography for evaluation of the heart were performed by physicians both *in vivo* and *ex vivo* in a canine model in the late 1970's and early 1980's. The first experimental study to use computed tomography for visualization of the heart and iatrogenically induced regions of myocardial infarction was performed in dogs in 1976. [31] This study utilized the prototype of the EMI CT 5000 body scanner. Images of the canine heart were acquired in two groups of patients. The first group had image acquisition performed during general anesthesia. All images in the second group were acquired post mortem. However, the second group was subdivided into those who where imaged immediately following intravenous contrast medium administration and euthanasia and those who where imaged without receiving intravenous contrast medium. It was determined that the slow acquisition rate of computed tomography technology at the time, resulted in motion artifact from the continuous beating of the heart, causing severe blurring of the heart and subsequent indistinction of its internal structures. Resultant cardiac images from the living canine

patients were described as a composite image of the heart obtained over several heartbeats.[32,33] The study also demonstrated that in the unmoving heart, the myocardium, cardiac chambers, papillary muscles and interventricular septum could be easily identified both with and without the presence of intra-cardiac contrast medium. The images acquired following intravenous contrast medium administration also permitted delineation of regions of normal myocardium from that of infarcted myocardium, which was subsequently confirmed with histologic evaluation.[31] Shortly thereafter, several other *ex-vivo* cardiac computed tomographic studies were performed in dogs, confirming that internal structures and myocardial infarctions could indeed be visualized in the quiescent heart.

In 1980, a group from the University of California established that computed tomography could be used for quantitative studies of the canine heart when they demonstrated that interventricular septal thickness could be reliably measured following intravenous contrast administration *in vivo* without the use of ECG gating.[33] A second group, Doherty et al, also determined that non-ECG gated contrast enhanced computed tomography could be effectively utilized to evaluate regions of myocardial infarction. However, when quantitatively compared to the restrospectively gated studies, the image quality was admittedly inferior. [34] Barter et al found during their evaluation of myocardial infarctions in a group of 10 humans, that it was possible to obtain CT images of the myocardium, cardiac chambers and great vessels with clarity, despite the lack of ECG-gating. Not only were they successful at diagnosing myocardial infarction, they were also able to detect the presence of hypertrophic cardiomyopathy and intra-ventricular thrombosis.[35]

Once it became clear that computed tomgraphy could be utilized to non-invasively and discriminately evaluate the heart, the future potential of this imaging modality was recognized. It also became clear that to optimize cardiac imaging, the obstacle of continuous cardiac motion would need to be overcome. Two solutions were put forth to deal with the inherent cardiac motion, the first was the synchronization of tomographic data acquisition to the cardiac cycle and the second was substantially decreasing CT data acquisition times. [31] [29,36]

Even with ECG gating, before the introduction of 256 and 320 MDCT, CT coverage of the heart during a single rotation of the gantry was incomplete. ECG-gated volume images of the heart consist of several image slabs reconstructed from data acquired in multiple consecutive heart beats. The result of incomplete cardiac coverage with single slice, 4, 16 and 64 MDCT is stair step artifact that can be present on multiplanar reconstructions or 3D volume rendered displays. This artifact is a result of changes in cardiac position and small variations of cardiac motion between cardiac cycles that occurs during each gantry rotation.[25] Further, ECG gated studies can be affected by the presence of arrhythmias and high heart rates. Ideal cardiac imaging can now be performed since the introduction of 256 MDCT, which allows complete cardiac volume coverage and image acquisition of the heart during one heart beat.

Image Quality

Many factors contribute to overall image quality including image noise, slice thickness, low contrast resolution, high contrast resolution, mA, rotation speed, kVP, pitch and reconstruction algorithm. Several of these factors are interrelated and can influence both image quality and each other.

Image noise

Quantitatively, image noise can be measured by the standard deviation of voxel values in a homogeneous medium. Often times, to determine the inherent noise of a system, a water phantom is employed. Parameters that influence image noise include mA, kVp, exposure time, slice thickness, reconstruction overlap, reconstruction algorithm and pitch. Other factors can also contribute, such as detector efficiency, but play a lesser role. [3]

Reduction of the mAs causes an increase in image noise by $\mathbf{1 / \sqrt{\Delta mAs}}$.[37] Many of the other factors that influence image noise are manifestations of change in the photon interaction with the detectors that have a similar effect as decreasing the mA (ie. decreased exposure time, decreased slice thickness and increased pitch).

Slice thickness

In single slice CT, X-ray beam collimation at the isocenter of the gantry determines slice thickness. In MDCT, detector width and the binning of the detectors largely determine slice thickness. In both conventional and helical CT, slice thickness is the greatest influencing factor for determining z-axis spatial resolution. However, with helical CT, pitch and the selected reconstruction algorithm also play a small role in defining z-axis spatial resolution.

To begin the discussion of slice thickness, the terms nominal slice thickness and effective slice thickness must be introduced. Nominal slice thickness is the slice width that is selected by the user and is applied to both axial and helical CT. Effective slice thickness is not a pre-selected number. Effective slice thickness is a result of the interpolation of the acquired measurement data in the longitudinal direction that is

required to generate a complete CT data set when utilizing helical CT acquisition. Due to the difference in data acquisition, conventional axial CT does not rely on interpolation of the data to have a complete data set for each image slice generated and as a result, the nominal and effective slice thicknesses are identical. This is best demonstrated by evaluation of the slice sensitivity profiles (SSP) for both types of CT acquisitions. The SSP shows the relative contribution of the anatomy along the Z-axis of the reconstructed image.[38] The SSP for images acquired with axial computed tomography has a trapezoidal contour with almost vertical margins. When related back to the anatomy that is being represented, a SSP with a trapezoidal shape reflects margins of an image slice that are sharply defined. Small structures are likely to be completely included or excluded in the slice and therefore more accurately represented. A helical image acquired with a pitch of 1 has a similar nominal and effective slice thickness as an axial image when measured at its full width half max (FWHM). However, the profile of the SSP is different, having a more bell-like contour with margins that taper at the edges. As the pitch is increased in helical CT the SSP and FWHM continue to increase in width, reflecting the inclusion of anatomic structures that are outside the nominal slice thickness in the reconstructed image.[38]

A slice sensitivity profile that has long far-reaching tails causes degradation of z-axis resolution.[39] In helical CT, the effective slice width is typically full width half max of the slice sensitivity profile.[25] Pitch also directly influences z-axis resolution by this same phenomenon. As pitch is increased, the shape of the slice sensitivity profile widens, again causing the effective slice thickness to increase, resulting in an overall decrease in spatial resolution. Specifically related to cardiac computed tomography, submillimeter spatial resolution is necessary both in-plane and longitudinally, along the z-axis to be

able to view small cardiac structures, such as the coronary arteries. When the in- plane and z-axis resolution are the same, the resolution is said to be isotropic. Isotropic imaging series are ideal as they allow reconstruction of the image in any plane without loss of spatial resolution or evidence of artifact.

Spatial resolution

Spatial resolution is another aspect of CT that initially limited the ability to visualize small cardiac structures, such as the coronary arteries. Spatial resolution, is classically defined as the ability of an imaging system to distinctly depict two objects as separate as they become smaller and closer together. The ability of an imaging system to be able to depict very small structures as being individual implies that this modality has high spatial resolution. High spatial resolution is required for evaluation of small anatomical structures. Spatial resolution, as it applies to multidetector computed tomography is affected by a large number of factors. In-plane spatial resolution is influenced by focal spot size, image matrix size, field of view, detector width and the reconstruction algorithm. Large focal spot sizes result in a greater degree of geometric unsharpness (penumbra) in the resultant image, therefore decreasing spatial resolution. The typical image matrix size utilized in computed tomography is 512 x 512. When the matrix size is maintained at 512 x 512, the field of view can be changed, thus directly affecting the pixel size. A small field of view would result in smaller pixels, or higher spatial resolution, than a larger field of view.

Contrast resolution, also known as low contrast resolution of a system can be determined by using phantoms that contain objects that have a small difference in density when compared to the surrounding medium. The ability to differentiate

structures that are similar in density from each other implies that the contrast resolution of the system is high. The mA, degree of image noise, slice thickness, reconstruction algorithm, window and level settings influence the contrast resolution of the system. Contrast resolution of CT far exceeds other modalities that rely on x-rays for image production. The contrast resolution of screen-film radiography is approximately 5% whereas it is approximately 0.5% in CT.[22]

Overall, CT has lower in plane spatial resolution when compared to traditional screen-film and digital radiography (approximately 7 line pairs (lp) per millimeter and 4 lp/mm, respectively). Seven line pairs per millimeter is approximately equivalent to a spatial resolution of 2mm.[24] Whereas CT has a spatial resolution of 1 lp/mm.[22]

Pitch

Before the advent of multidetector computed tomography, pitch, also known as beam pitch or collimator pitch, was a way to describe the rate of scan acquisition. A high pitch indicates a fast scan time. Whereas a low pitch is indicative of a slower overall scan time for the same z-axis coverage. Beam pitch is defined as table travel per complete rotation of the gantry divided by the X-ray beam width. With the advent of MDCT scanners, a second definition of pitch was introduced, called the detector pitch. It is defined as the table travel per complete rotation of the gantry divided by the data acquisition width of each slice.[22,30,40] Use of this term is variable and for the sake of clarity, most have disregarded it in favor of the original term. In MDCT, the x-ray beam width is calculated by multiplying the number of active channels during the scan, by the width of the detector of each data acquisition system.[41] With a pitch of "0", there is no table motion and scanning is axial. With a pitch of 1, table displacement for each

rotation is equal to the z-axis dimension of the array of active rows of detectors. A pitch greater than 1 implies gaps in the helix of projections, whereas a pitch between 0-1 implies overlap between the projections.[30] For cardiac scanning, a pitch within the range of 0.2-0.4 is typically utilized.[41] Many modern CT scanners are equipped with automated pitch adaptation based on the patient's heart rate so that there is slight overlap of the data collected to ensure that there are no gaps in the image data collection and also to improve longitudinal resolution.[24] To a small degree, pitch can influence overall spatial resolution. As pitch is increased, scan time is decreased. This results in an increase in image noise, thus making distinction of fine anatomic details more challenging. To compensate for this, mAs can be increased causing an increase in the number of photons striking the CT detectors.[3]

Image Reconstruction

Images are reconstructed from linear interpolation of projection data from rays that are the closest to the image plane. A minimum of 180 degrees of projection data are mathematically required to reconstruct a complete image slice. Effective slice thickness is increased as a consequence of increasing pitch, due to the need for linear interpolation of the projection data. [30]

Cardiac Gating

The second method for increasing temporal resolution, as it applies to cardiac imaging, is ECG gating. ECG gating was pioneered through the collaborative effort of scientists and physicians that collectively contributed to its development at the Mayo Clinic in the mid 1970's. The impetus for such work was the introduction of cardiac

surgery in the 1950's and the necessity to develop a non-invasive imaging modality that could accurately characterize cardiac pathology pre-operatively.[36] Two types of cardiac gating have been developed, retrospective ECG gating and prospective ECG gating. In retrospective ECG gating the image acquisition can occur throughout the R-R interval. With prospective ECG gating, the image acquisition occurs at a predefined time point. For the purpose of cardiac CT, the R-R interval of the cardiac cycle is divided into many segments, each representing a defined interval of the cardiac cycle. The first R wave is the 0% time point at end diastole, the next R wave is the 100% time point of the first cardiac cycle and the 0% time point of the next cardiac cycle. [3] The heart and coronary arteries are most quiescent during end-systole and mid- to end diastole. Acquisitions at the end of systole/early diastole (10-30% of the cardiac cycle) and immediately before atrial contraction (beginning 80% of the cardiac cycle), result in more image artifacts than do acquisitions at mid-diastole. [42]

Prospective ECG Triggering

Prospective ECG triggering, initially developed for electron beam CT technology, has been adapted to MDCT technology. Prospective ECG triggering is reliant on axial scanning, where each volume of data is acquired incrementally before the table travels to the next region of the heart in the z-direction. [3] Utilization of this technique requires that the patient's ECG signal be monitored throughout the CT scan. The start of the diastolic phase of the cardiac cycle is estimated from the prior three to seven consecutive heart beats.[30] During prospective ECG triggering, image data is acquired during the short period of the R-R interval that was pre-selected. During the remainder of the cardiac cycle, the radiation being emitted from the X-ray tube is

significantly decreased or off, significantly reducing exposure to the patient. The acquisition can be either relative, being defined as a certain percentage of the R-R interval time or absolute and defined by a set time in milliseconds. [25] Acquisition can only be targeted at one phase of the cardiac cycle, typically diastole, which occurs between 70-80% of the R-R interval.[19] A volume image of the heart consists of several image slabs reconstructed from axial scan data acquired in multiple consecutive heart beats. The number of axial images within an image slab corresponds to the number of active detector slices. [25] Several studies have demonstrated that the ideal R-R interval can be variable, depending on the structure of interest. Hong and Becker et al. found that when using prospective triggering to evaluate the coronary arteries that different R-R interval trigger delays were required to obtain the maximum image quality for the right coronary artery (50%) and left circumflex (60%), while the left anterior descending had optimal image quality at 50% and 60% trigger delay.[42] Kopp et al. also evaluated the coronary arteries utilizing retrospective ECG gating. They found that each the optimum reconstruction windows for the left anterior descending, left circumflex and right coronary arteries were variable. Suggesting that for some cardiac structures, a single reconstruction window or trigger point may not be ideal for evaluation of the heart in its entirety. They also indicate that because of their position in the coronary groove, the right coronary artery and left circumflex artery have more rapid diastolic motion than does the left anterior descending artery. The motion is caused mainly by atrial contraction during end diastole. [27]

Well established limitations of prospective ECG triggering include arrhythmias and changes in heart rate. With prospective ECG triggering, the estimate of the next R-R interval may be wrong due to subsequent change in heart rate or rhythm. Hong and

Becker found that patients with higher or irregular heart rates had poorer image quality, when compared to patients that had a heart rate less than 75 beats per minute, which they attributed to inappropriate trigger selection. [42]

In early CT scanners, in order to achieve a complete scan through the heart during a single breath hold, spatial resolution was limited by the presence of fewer number of detectors in the z-axis and the necessity of utilization of maximal allowable slice thickness. However, with the increase in detector number in the z-axis and subsequent ability to have greater volume coverage with decreased slice thickness in modern CT scanners, this is no longer a constraint. [30]

Lastly, when prospective ECG triggering is utilized, data is not acquired throughout the entire cardiac cycle for the entire volume of the heart. This limited data set prevents the raw data from being used for functional evaluation of the heart, where all regions of the heart must be represented over the entire cardiac cycle in order to produce 4-dimentional images.

Retrospective ECG Gating

Retrospective ECG gating allows acquisition of image data and image reconstruction at any precise time point during the entire cardiac cycle. When utilizing retrospective ECG gating, image data is acquired throughout several cardiac cycles, while the ECG signal of the patient is being simultaneously recorded. The data from each individual cardiac cycle is subsequently divided into defined segments, spanning the 0%-100% points of the cycle based on the time lapsed from the beginning of each R-R interval. Algorithms are then used to sort the data from different phases of the cardiac cycle. [3] Retrospective ECG gating does not rely on estimation of the presumed next R-

R interval. Reconstruction data intervals can be accurately measured on the basis of the actual R-R intervals that occurred during scanning. With retrospective ECG gating, the final reconstruction is based only on the images obtained during a portion of the cardiac cycle, typically mid-diastole, with the reconstruction point selected according to the actual heart rate. This method greatly reduces cardiac motion. To have the freedom to be able to reconstruct the image data at any interval of the cardiac cycle, every position of the heart must be covered by a detector row at every point in the cardiac cycle. This means that the scanner table must not advance more that the total width of than active detectors for each heart beat. Helical pitch can be varied proportionally to the heart rate to achieve continuous volume coverage. Typical pitch for an average heart rate of 70 beats per minute is 0.3:1.[30] When utilizing retrospective ECG gating, functional evaluation of the heart can be performed because all segments of the cardiac cycle are imaged.

Chapter 2: Materials & Methods:

MDCT cardioangiography was performed on six healthy research canines following a protocol approved by the institutional animal care and use committee. At the onset of the study, each patient had a physical exam, complete blood count, biochemistry, urinalysis, electrocardiogram and echocardiogram performed. The latter two procedures were performed by a board certified veterinary cardiologist. The time interval between complete lab work, echocardiographic studies and the time of CT examinations was no greater than 45 days. The median patient weight was 10.2 kg. On the days of their anesthetic events, the patients had a second physical exam and an abbreviated set of blood work performed, which included a packed cell volume (PCV), total solids (TS) and an Azostick to ensure the normal hydration and renal status of the patient.

The study utilized a double cross-over study design, in which each of the six dogs had two CT cardiac studies, a non-ECG gated CT acquisition performed at the veterinary teaching hospital using a 16 MDCT scanner[Δ] and a retrospective ECG gated acquisition performed at a local human hospital using a 64 MDCT scanner[Ψ]. In total, each patient had 2 anesthetic episodes and two CT acquisitions. A schedule of the 12 CT scans was designed to accommodate the patient usage restrictions.

Both non-ECG gated and ECG gated post contrast scans were acquired following induction of bradycardia with a specifically designed anesthetic regiment. The protocol for CT studies performed using the non-ECG gated 16 MDCT was as follows:

[Δ] Toshibia Aquilion 16, Toshiba American Medical Systems Inc., Tustin, CA

[Ψ] LightSpeed VCT 64 MDCT, GE HealthCare, Waukesha, WI

patients were positioned in sternal recumbency. Preceding all CT acquisitions, hyperventilation was performed to induce apnea, preventing motion artifact secondary to respiration. An initial non-contrast scan was performed to ensure adequate z-axis coverage from the base of the heart through its apex. Following this, a timing bolus of 5ml of contrast medium[δ] was administered at a rate of 0.8ml/s, using a single barrel pressure injector[Ω]. Contiguous single axial scans were performed every 2 seconds at the level of the left ventricle, where a ROI had been set to monitor contrast medium density values. This allowed determination of the time of maximum contrast enhancement in the left ventricle. Time of peak left ventricular enhancement was used to determine time to scan through the heart following administration of the parent bolus of intravenous contrast medium. Scanning after the parent bolus entailed acquisition of a series of 5 contiguous CT scans performed through the heart. Contrast medium was administered at 2.2ml/kg and followed by a 2.2ml/kg chaser bolus of physiologic saline administered with the pressure injector at a rate of 0.8ml/s. These scans were acquired in helical mode with a kVp of 120 and a mAs of 300, gantry rotation time of 350ms, slice thickness of 1 mm and a smooth convolution kernel. Heart rate and blood pressures were recorded for each scan through the heart. A similar protocol was used when scans were performed with the 64 MDCT equipped with retrospective ECG gating. However, instead of having 5 contiguous scans following the parent bolus of contrast medium, a single helical scan was performed through the heart. Parameters for the 64 MDCT were a kVp of 100, mA of 300, pitch of 0.219, slice thickness of 0.625mm and a standard convolution kernel.

[δ] Ultravist 370, Bayer HealthCare Pharmaceuticals , Berlin, Germany
[Ω] Stellant, Medrad, INC., Warrendale, PA

A standardized anesthetic protocol was designed to achieve bradycardia and was implemented by a board certified anesthesiologist for all CT acquisitions. Premedication consisted of acepromazine (0.05mg/kg) and butorphanol (0.3 mg/kg) administered intraveneously. Anesthetic induction was attained with intravenous propofol (8mg/kg) administered to effect. Each patient was then maintained on 2-3% isoflurane and 100% oxygen. Lactated ringer solution was administered at a rate of 10 mL/kg/hr. One patient received a dopamine constant rate infusion of 5ug/kg/min in 0.9 NaCl to maintain a mean arterial blood pressure greater than 70 mmHg. After achieving a steady state of anesthesia, a pre-contrast scan was performed. Following this, bradycardia, with a target heart rate of 40-60 bpm, was induced. Initially, the bradycardic state was induced with a single 3 ug/kg intraveneous bolus of dexmedetomidine, which could be repeated if bradycardia was not achieved. However, the second patient became refractory to the dexmedetomidine and in order to induce bradycardia, intravenous Fentanyl (3.15ug/kg IV) had to be administered. To avoid this in subsequent patients, the protocol was changed and bradycardia was induced by administering a 3ucg loading dose of dexmedetomidine followed by initiation of a dexmedetomidine constant rate infusion (7.5ucg/kg/hr). A single patient became refractory to the new protocol during one of their studies at the off site location and required propranolol given as a 0.2mg IV bolus to induce a bradycardic state. Two other off-site patients received esmolol as a CRI at 3mg/kg/hr prior to initiating the dexmedetomidine CRI to help achieve bradycardia. Following induction of bradycardia, the test bolus and series of cardiac acquisitions were performed. After successful completion of the CT scans, atipamezole was administered intramuscularly and the patient was recovered from anesthesia.

Postprocessing of the retrospective ECG gated data for each patient, included dividing the R-R interval of the cardiac cycle into the maximal number of increments allowable. The calculation of increment value was based on number of slices generated during the cardiac scan and limited by the maximum series size allowable by the software and ranged from 4-6%. Image quality was assessed for 21 cardiac structures in each of the post-contrast scans performed using consensus agreement of two radiologists and a radiology resident. Images of the cardiac structures were assessed in the transverse plane. Each transverse slice that included the structure of interest was assessed to determine the presence of motion. A score of "0", "1" or "2", representing the degree of cardiac motion present, was assigned for each structure. A score of "0" was assigned when motion artifact rendered the image non-diagnostic, therefore preventing critical evaluation and interpretation of the morphologic structures present. A score of "1" was assigned when motion artifact was present, but did not prevent the image of the structure from being identified and critically evaluated. A score of "2" was assigned when the cardiac structure was identified clearly without evidence of motion artifact.

Image quality was further assessed by evaluating the number of scan slices for each of the 6 scans for each of the 6 patients, that demonstrated motion artifact. Percentage of motion for each scan was then calculated.

Statistical programming/Analysis:

SAS (version 9.2) macros were generated and extensively used to analyze the data as follows: 1) Examine each record in the dataset (combination of dog and scan) and count the number of structures (out of 21) with a score of 1 or 2 (diagnostic scan scores). 2) For the non-ECG gated scans, generate a complete permutation of the 5 sequences

performed for each dog. This was performed because motion was thought to be independent of scan order. The permutation generated 120 sequences within each dog, for a total of 720 dog-sequences over all the 6 dogs. These dog sequences were subjected to the SAS program and used to estimate the likelihood (probability) of achieving diagnostic quality images of 21 cardiac structures at each scan number. Statistical significance was set to $\alpha < 0.05$.

Chapter 3: Results

Each patient's single ECG-gated MDCT scan was of high diagnostic quality, resulting in quality scores that were almost exclusively 2, therefore generating diagnostic images for all of the 21 cardiac structures evaluated. The sequence of 5 non-ECG gated MDCT scans for each patient also resulted in images of the cardiac structures that were of diagnostic quality, meaning they achieved a quality score of 1 or 2. However, the individual scans were of variable quality, and a complete set of diagnostic images for all 21 structures was not achieved from an individual scan. Thus it required more than one scan through the heart to generate a set of diagnostic images of all 21 structures.

The average number of scan acquisitions needed to obtain a diagnostic image of a specific cardiac structure during a single non-ECG gated scan was determined based on the 720 dog-sequences. Grouped permutation of the quality scores from all 5 scans within a dog (30 scans total) was performed because the quality score was felt to be dependent on cardiac motion present at the time of the scan, and is not dependent on the chronological scan order. Thus by using all of the 120 possible sequences generated for each patient, the average number of scans needed to achieve diagnostic quality was able to be determined. The minimum number of scans needed to visualize each of the individual 21 cardiac structures was generated. If the minimum number of scans needed to identify the structure was not an integer, the next larger integer was assigned, ie., if the average number of scans needed to visualize a structure was 1.6, the scan number assigned was 2. This data is represented in order of decreasing difficulty in **Figure 1**. It is evident that some of the 21 anatomic structures are more difficult to image using non-ECG gated CT. This is largely attributed to a greater degree of inherent cardiac

motion in the structures and is reflected in the greater number of scans needed to acquire a diagnostic image of the structure. Differences in difficulty in achieving diagnostic images of the right coronary artery, left circumflex artery, left septal branch and left paraconal branches of the left coronary artery were compared using analysis of variance. It was determined that there was no significance difference ($p>0.05$) in degree of difficulty in acquiring diagnostic images of these four structures.

The 720 dog-sequence data was used to determine the probability of achieving diagnostic quality images of all 21 cardiac structures after each of the 5 cumulative scans. Therefore determining the total number of scans necessary to be able to achieve a diagnostic image of all the cardiac structures evaluated. This cumulative diagnostic value data is represented in **Figure 2**. Scans acquired using the 64 MDCT ECG-gated CT unit had a diagnostic value of 100% for each individual scan performed for each patient. Representative images of the 21 cardiac structures evaluated and their corresponding diagnostic quality scores are shown in **Figures 3-24.**

Calculation of the total average percent motion for all of the 16 MDCT non-ECG gated acquisitions was performed. This data was based on the 30 MDCT non-ECG gated series (5 series on each of 6 dogs). A student's t-test was used to compare the total percent motion for the 16 slice MDCT to the average percent motion calculated for the scans acquired using the 64 MDCT non-ECG gated unit ($n=6$). The mean percent motion calculated was 46.85 for the non-ECG gated studies. A percent motion of "0" was calculated for the ECG-gated studies. A significant difference ($p< 0.01$) in percent motion was demonstrated between the non-ECG gated and the ECG gated studies.

Chapter 4: Discussion

Numerous investigators have demonstrated the reliability and diversity of applications of ECG gated 16 and 64 MDCT for the evaluation of cardiac pathology in the human patient.[18,19,21,43-45,46,47] It was only recently that demonstration of prospective ECG gated computed tomography as a diagnostic tool utilized in the canine patient was published.[6] Although few clinical and research oriented human cardiac CT studies are performed without the benefit of ECG gating, this cardiac imaging software is not generally included with the standard imaging software package that is included with the purchase of a CT unit. This can lead to a significant increase in the overall cost of a CT scanner. Though published data concerning the prevalence of CT units equipped with ECG gating software within veterinary community is not available, it is suspected that the additional cost of this software and the lack of recognized utility of gating software are largely responsible for its limited use in this capacity to date. The gross disparity that exists between the utilization of cardiac computed tomography in human and veterinary medicine and the observation of visualization of normal cardiac structures on routine non-cardiac CT scans was the impetus behind conducting this experimental study.

Evaluation of overall percent motion present in non-ECG gated versus ECG gated CT scans of the heart dramatically demonstrated the distinct difference in the presence of cardiac motion that is evident without selective reconstruction of cardiac images from cardiac diastole. The disparity of cardiac motion between the two methods clarifies the benefit of utilizing ECG gating software to optimize cardiac images. Evidence of this is further demonstrated in the diagnostic image quality results from the 6 individual ECG gated and the serial non-ECG gated CT acquisitions.

As anticipated, the scans acquired while utilizing retrospective ECG gating were of excellent diagnostic quality. Each of the 21 cardiac structures evaluated could be identified on each scan reliably, without evidence of motion artifact related to cardiac contraction. Image quality did not vary with minor fluctuations in heart rate. It has been demonstrated that retrospective ECG gated software provides cardiac images of high diagnostic quality with heart rates that approximate, or are less than, 65bpm. Continued improvement in image quality from initial 4 and 16 MDCT units to the 64 MDCT is largely attributed to concurrent technological improvements in both temporal and spatial resolution of the newer generation of CT scanners.[48]

Quantitative evaluation revealed that after 5 contiguous non-ECG gated scan acquisitions through the heart, diagnostic images of all 21 cardiac structures could be obtained for each patient. Although diagnostic scores were only reported for structures visualized in the axial plane, findings were subjectively similar when multi-planar reconstructed images were viewed.

In these non ECG-gated studies, temporal resolution was limited by the minimum gantry rotation speed of the CT unit, pitch and the degree of bradycardia established in the patient during their scans. Although it is clear that cardiac motion cannot be completely alleviated with a bradycardic state alone, it did have a positive effect on overall image quality in our non-gated studies. Intentional induction of bradycardia allowed us to effectively prolong the diastolic phase of the cardiac cycle, helping reduce or eliminate motion artifact. It has been well established that patient heart rate influences the ability to acquire diagnostic images of the heart, especially the coronary arteries.[49] As heart rate increases, the duration of each cardiac cycle decreases and is manifested by both a decrease in the phase of contraction and relaxation.

However, the shortening of the cardiac cycle is non-uniform and the decrease in the length of the diastolic phase is greater.[50,51] The correlation of heart rate data and number of scans needed to obtain diagnostic images of all cardiac structures was not quantitatively evaluated. It is thought that with a progressive decrease in heart rate, a decrease in the number of cardiac scans needed to produce diagnostic images of all structures would also be observed. In humans, beta-blockers are routinely administered prior to CT evaluation of the heart if their heart rate exceeds 65bpm. The pharmacologic actions of ß-adrenergic receptor antagonists, are to cause a decreased heart rate a cause a sinus rhythm.[52,53] This allows for improved cardiac imaging.[54]

Although ß-blockers are commonly administered when CT angiography is performed in human patients, many adverse affects can occur including: excessive bradycardia and hypotension, worsening of heart failure and second or third degree heart block, anaphalaxis and bronchospasm.[52] Since similar adverse affects can occur in the veterinary patient, careful evaluation of the patient should be performed prior to administration.[53]

Cardiac structures at the base of the heart were more susceptible to cardiac motion. Those structures for which it was most challenging to obtain high quality images included the left paraconal branch of the left coronary artery, the circumflex branch of the left coronary artery and the right coronary artery. However, a significant difference in difficulty of imaging these structures was not found. Motion during the cardiac cycle has been extensively investigated especially with regard to the coronary arteries.[27,42,49]Our data is in agreement with observations in the medical literature that demonstrate the high degree of motion present in the coronary arteries which results in increased difficulty of obtaining high quality images of these small vessels with respect

to other cardiac structures. It has been demonstrated in humans, that during ventricular systole there is a decrease in the base-to-apex length. This is largely a result of motion of the base toward a relatively stationary apex. This greater degree of motion at the cardiac base, and high degree of coronary artery movement, contributes to the overall difficulty of imaging these structures.[51] In human patients, the right coronary artery is the most challenging of the coronaries to obtain high quality images of. This is secondary to the high velocity of motion it demonstrates during the cardiac cycle. Variation of coronary motion both within and between individual patients is thought to be an effect of cardiac shape, size and function.[55] Although we were working with canine patients that have obvious differences in conformation and cardiac morphology, the coronary arteries, similar to in human patients, were more difficult to achieve diagnostic images of, as demonstrated in Figure 1. This difference in difficulty is demonstrated by the increase in number of scans required to obtain diagnostic images of the coronary arteries.

One of the largest factors influencing the overall image quality in cardiac CT is patient heart rate. A heart rate range of 60-65 bpm has been correlated with good image quality that exhibits limited evidence of motion artifact. (Shim 2005) In this study, an anesthetic protocol specifically designed to achieve heart rates below 65 bpm was implemented. Modification of this anesthetic protocol was necessary as a result of persistently high patient heart rates achieved at the off-site CT location where ECG-gated studies were performed. It was suspected that this was secondary to catecholamine release experienced by the patients during transportation to the off-site location. Although these canine patients received sedation prior to leaving their boarding facility, they were not acclimated to vehicular transportation. When this same

group of patients was imaged onsite, without the need for vehicular transportation, they did not require additional beta-blockers to achieve and maintain a bradycardic state. Ultimately after pharmacological manipulation, a mean heart rate of 45 bpm was achieved for all patients.

There are several limitations to this study. Unlike cardiac computed tomography angiography performed in human patients, veterinary patients require general anesthesia for this procedure. This may preclude the use of CT for cardiac imaging in favor of echocardiography to evaluate the heart. In contrast to conventional angiography, which has a higher temporal resolution than computed tomography, the use of ß-blockers and alpha-2 agonists were utilized to induce bradycardia in this study. Utilization of these medications may be contraindicated in a subset of patients, making conventional angiography or echocardiography the preferred diagnostic test.

Non-ECG gated computed tomography angiography was performed in a patient population with an average heart rate of 45bpm. Increased heart rates may have resulted in overall decrease in image quality. Attaining such a degree of bradycardia may not be safe in some clinical patients.

Chapter 5: Conclusions

In our study, we were able to obtain diagnostic images for all cardiac anatomy evaluated with a non-ECG gated CT. However, this required multiple scans through the heart. Overall, the image quality scores were better on the ECG-gated scans, but diagnostic images were obtained on both scanners. Given the successful outcome of achieving diagnostic images of the heart when utilizing ECG gated and non ECG gated studies in bradycardic patients, further research exploring the utility of MDCT in canine cardiac imaging is encouraged. Translational applications of cardiac CT in dogs, such as successful imaging at higher heart rates and decreasing radiation dose, are obvious future research focus areas that would benefit pediatric human imaging. The results also support the ability for current veterinary institutions to use their current CT scanners, most without ECG gating, for imaging the canine heart for clinical cases.

	Structure	Mean number of scans	Minimum number of scans
1	Paraconal branch of the left coronary artery	1.74	2
2	Left circumflex coronary artery	1.64	2
3	Right coronary artery	1.53	2
4	Sinus of Valsalva and origin of the coronary arteries	1.39	2
5	Right atrium	1.39	2
6	Septal branch of the left coronary artery	1.38	2
7	Left atrium	1.23	2
8	Ascending aorta	1.20	2
9	Brachiocephalic trunk	1.16	2
10	Right auricle	1.15	2
11	Left auricle	1.15	2
12	Right ventricle	1.10	2
13	Main pulmonary artery	1.06	2
14	Aortic arch and descending aorta	1.03	2
15	Left subclavian vein	1.03	2
16	Right pulmonary artery	1.02	2
17	Pulmonary veins	1.00	2
18	Left ventricle	1.00	1
19	Azygous	1.00	1
20	Cranial vena cava	1.00	1
21	Left pulmonary artery	1.00	1

Figure 1. Mean and minimum number of scans needed to obtain a diagnostic image of each of the cardiac structures evaluated in the canine heart.

Scan	Cumulative percentage diagnostic scan
1	10%
2	51.67%
3	80%
4	93.33%
5	100%

Figure 2. Cumulative number of scans needed to obtain a diagnostic scan of all the cardiac structures evaluated in the canine heart.

a) Score 2

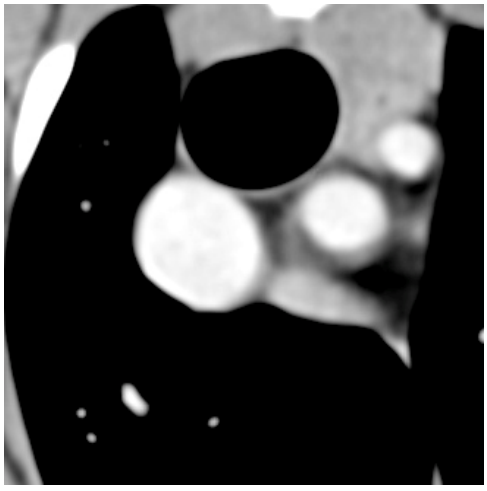

b) Score 1

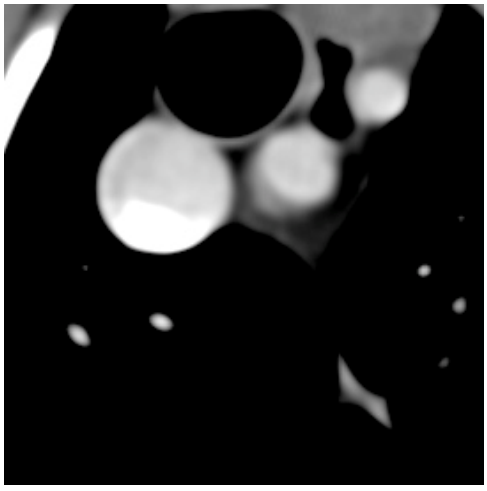

c) Score 0

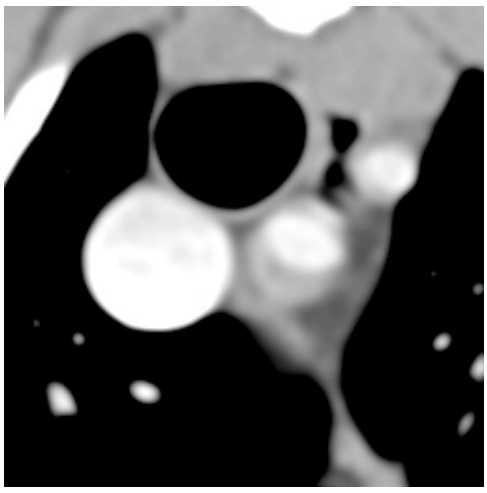

Figure 3. Transverse images at the level of the brachiocephalic trunk. a) Score 2 b) Score 1 c) Score 0

a) Score 2

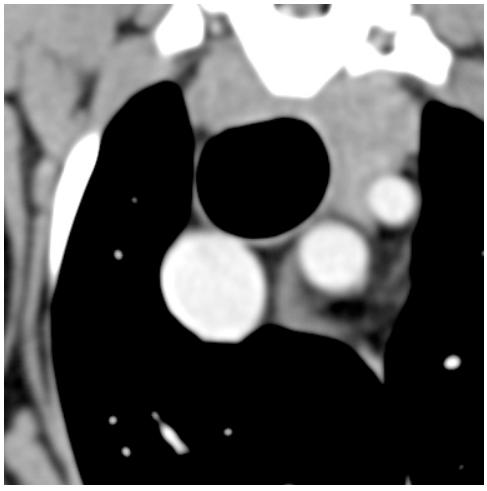

b) Score 1

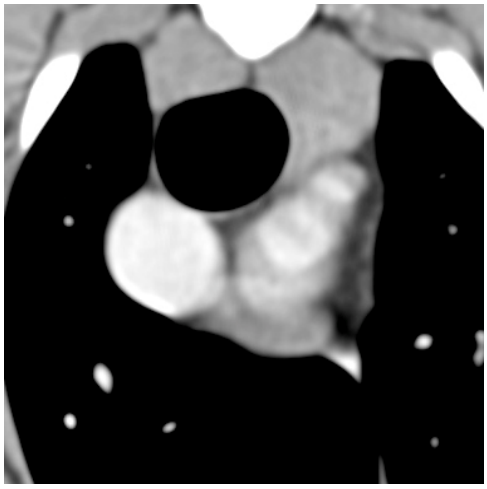

c) Score 0-N/A

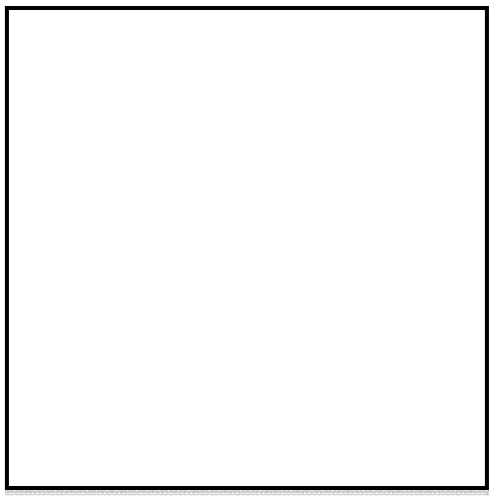

Figure 4. Transverse images at the level of the cranial vena cava.

a) Score 2

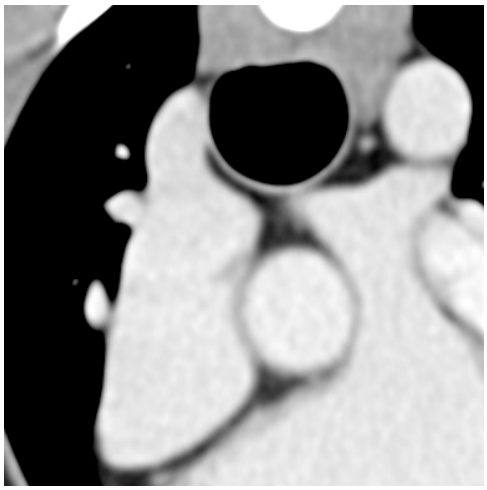

b) Score 1-N/A

c) Score 0- N/A

Figure 5. Transverse image at the level of the azygous vein.

a) Score 2

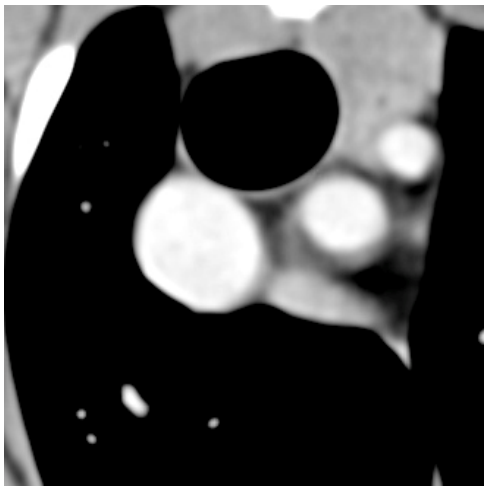

b) Score 1

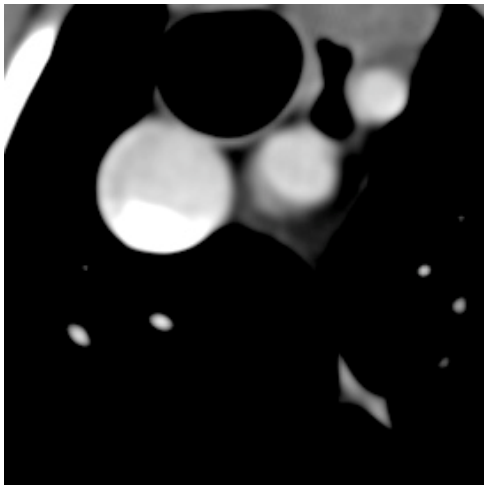

c) Score 0

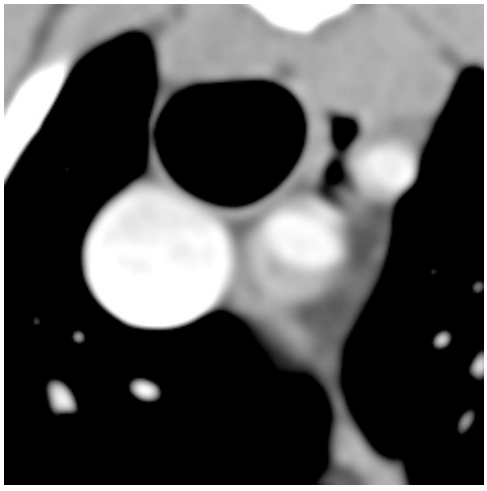

Figure 6. Transverse images at the level of the brachiocephalic trunk.

a) Score 2

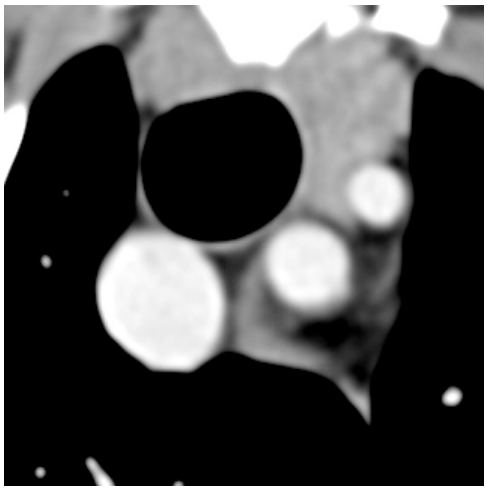

b) Score 1

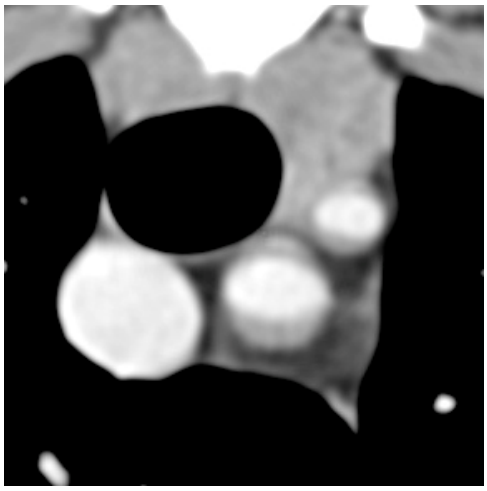

c) Score 0

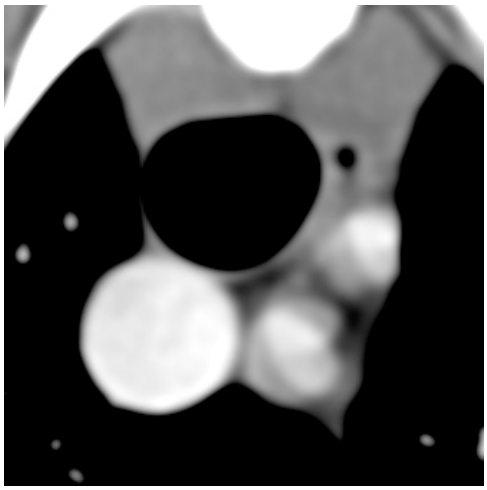

Figure 7. Transverse images at the level of the left subclavian vein.

a) Score 2

b) Score 1

c) Score 0

Figure 8. Transverse image at the level of the ascending aorta.

a) Score 2

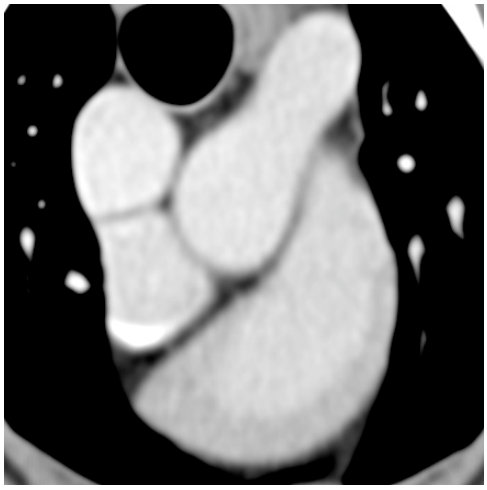

b) Score 1

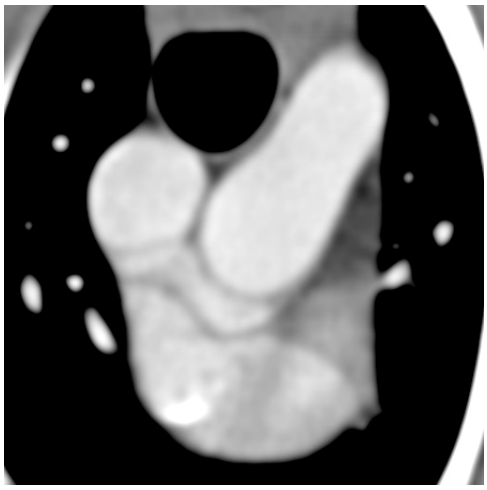

c) Score 0

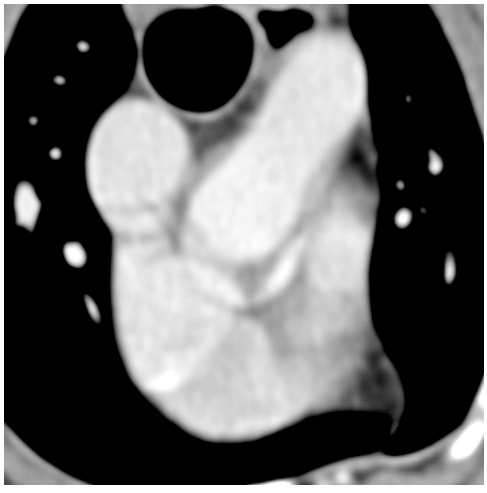

Figure 9. Transverse section of the aortic arch and descending aorta.

a) Score 2

b) Score 1

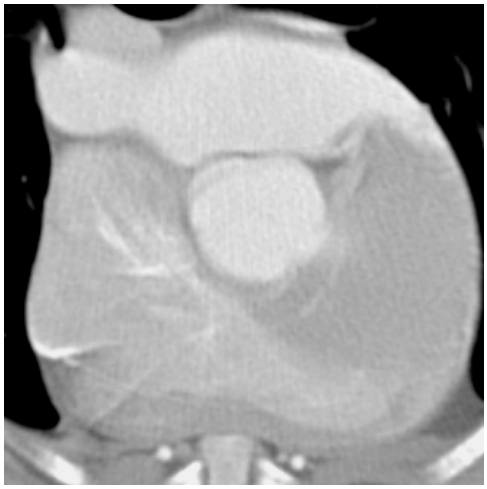

c) Score 0

Figure 10. Transverse images at the level of the sinus of valsalva and origin of the coronary arteries.

a) Score 2

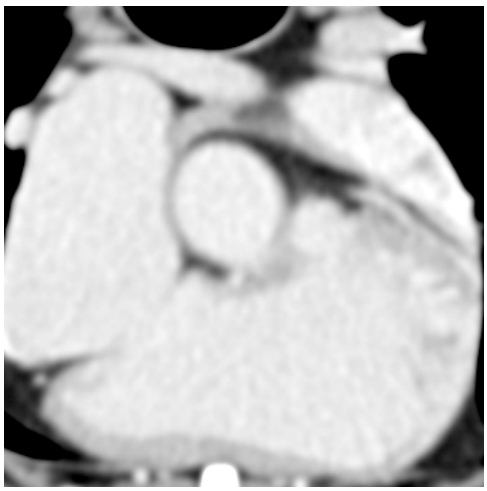

b) Score 1

c) Score 0

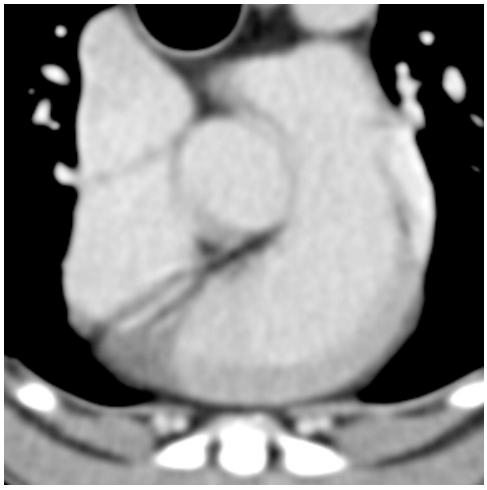

Figure 11. Transverse in ry artery.

a) Score 2

b) Score 1

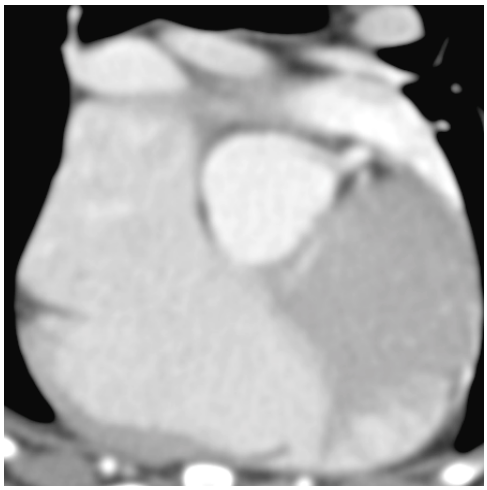

c) Score 0

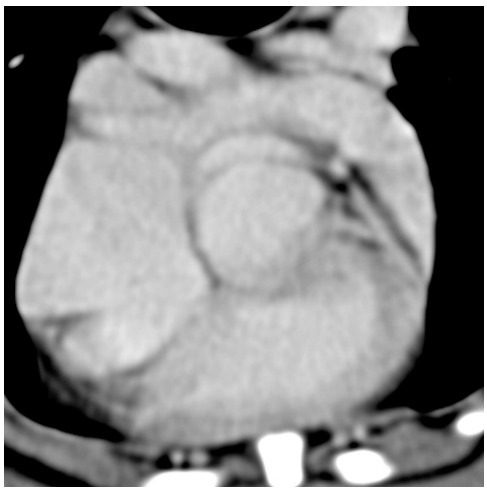

Figure 12. Transverse in[illegible]ex artery.

a) Score 2

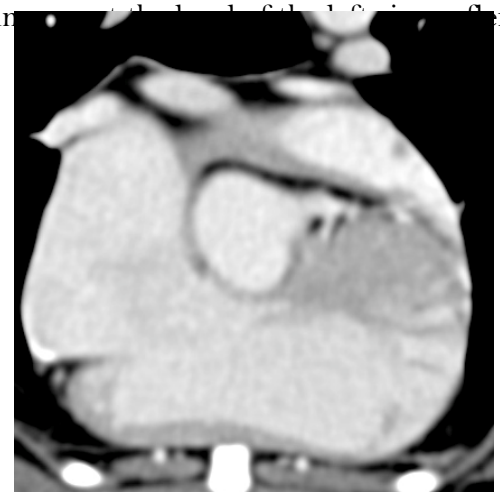

b) Score 1

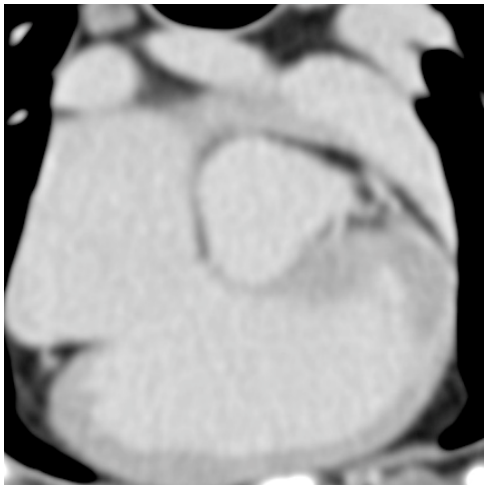

c) Score 0

Figure 13. Transverse images at the level of the septal branch of the left coronary artery.

a) Score 2

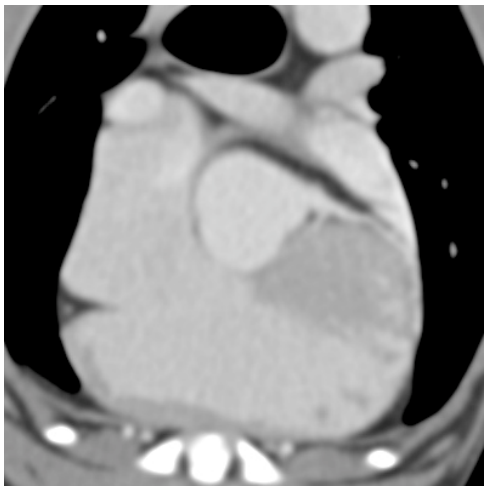

b) Score 1

c) Score 0

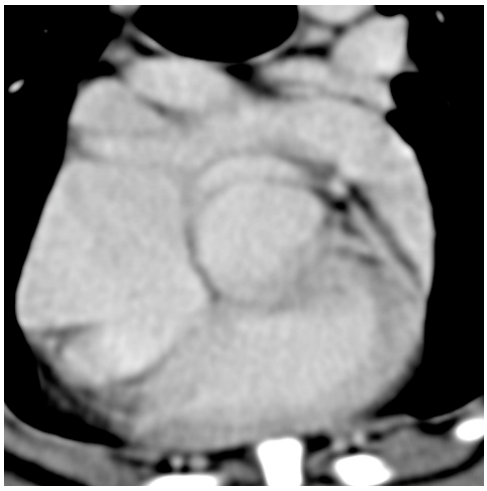

Figure 14. Transverse images of the paraconal branch of the left coronary artery.

a) Score 2

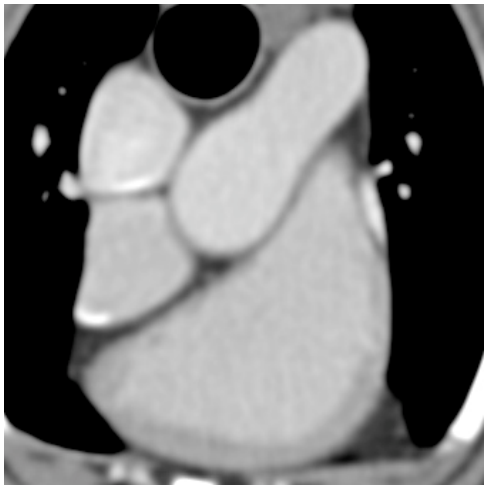

b) Score 1

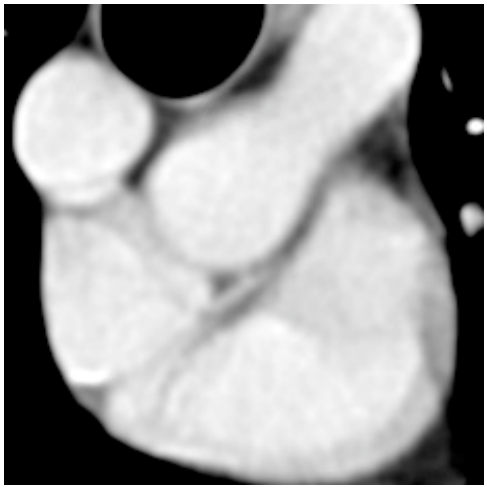

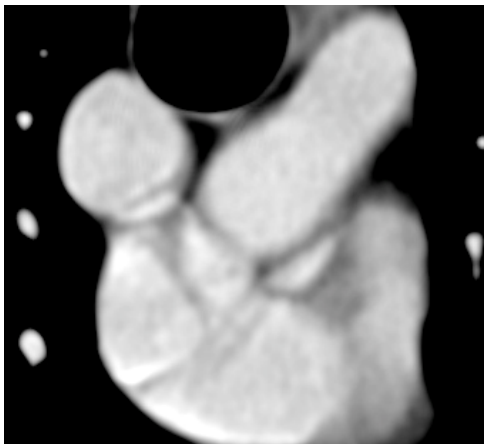

c) Score 0

Figure 15. Transverse images at the level of the right auricle.

a) Score 2

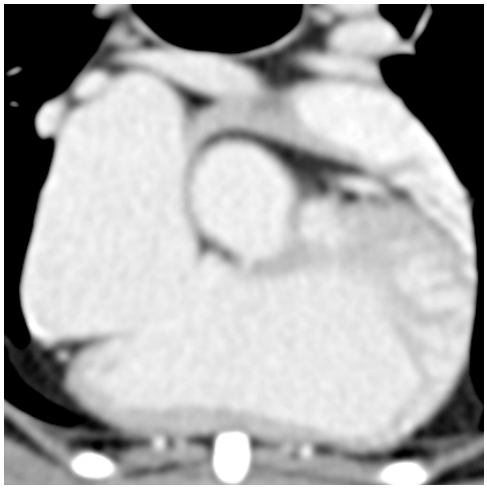

b) Score 1

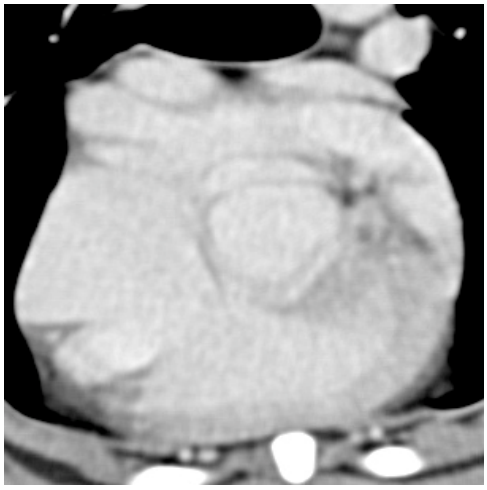

c) Score 0

Figure 16. Transverse images at the level of the right atrium

a) Score 2

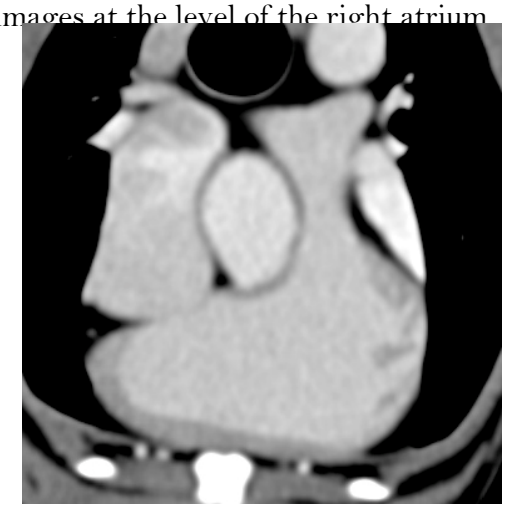

b) Score 1

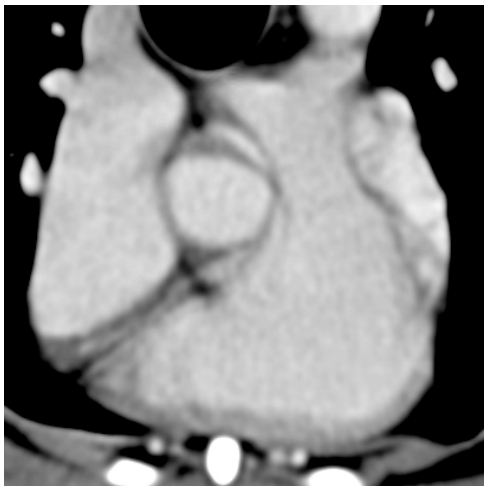

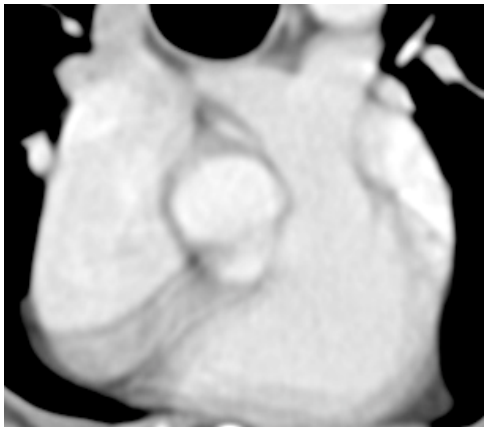

c) Score 0

Figure 17. Transverse images at the level of the right ventricle.

a) Score 2

b) Score 1

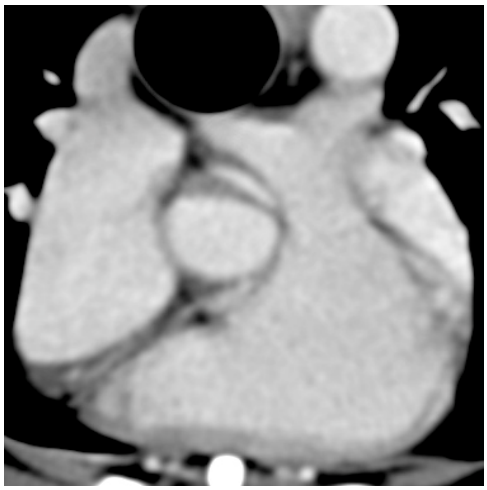

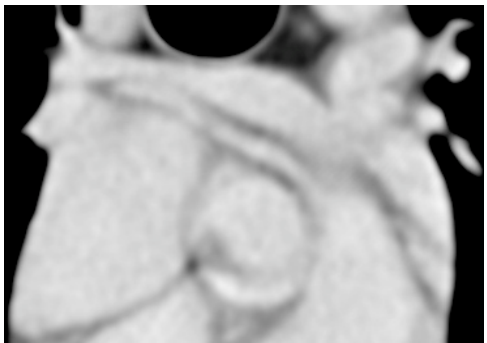

c) Score 0

Figure 18. Transverse images at the level of the main pulmonary artery.

a) Score 2

b) Score 1

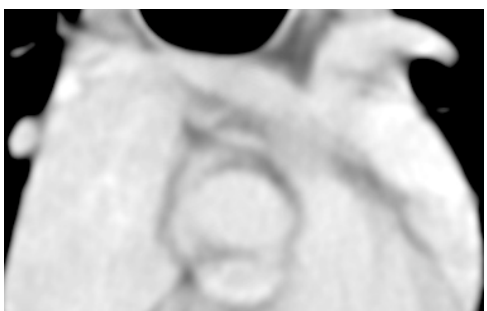

c) Score 0

Figure 19. Transverse images at the level of the right pulmonary artery.

a) Score 2

b) Score 1

c) Score 0-NA

Figure 20. Transverse images at the level of the left pulmonary artery.

a) Score 2

b) Score 1

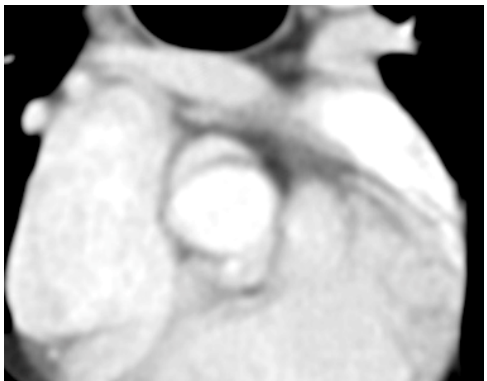

c) Score 0

Figure 21. Transverse images at the level of the left auricle.

a) Score 2

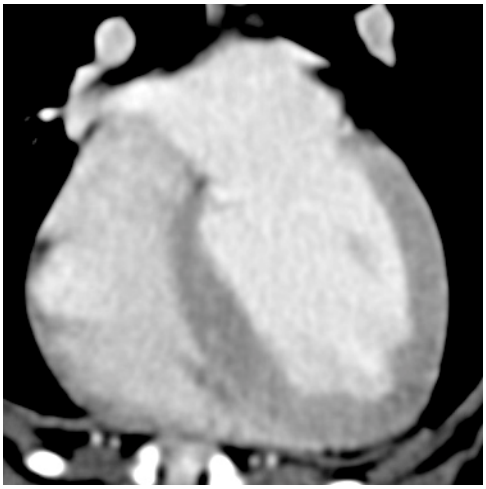

b) Score 1

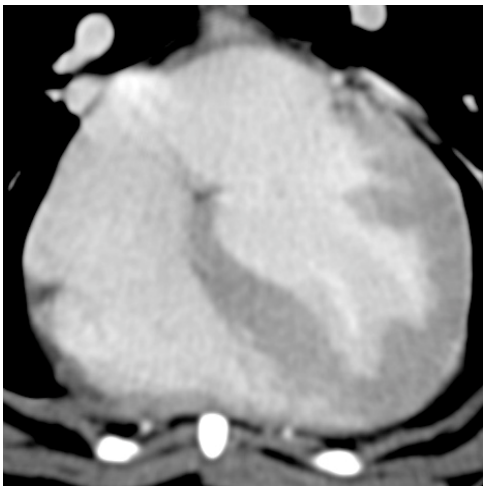

c) Score 0

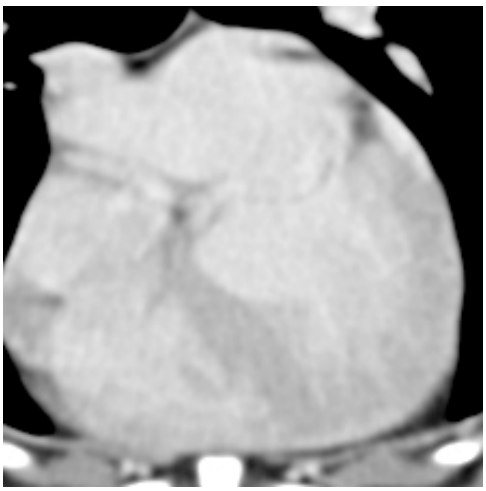

Figure 22. Transverse images at the level of the left atrium.

a) Score 2

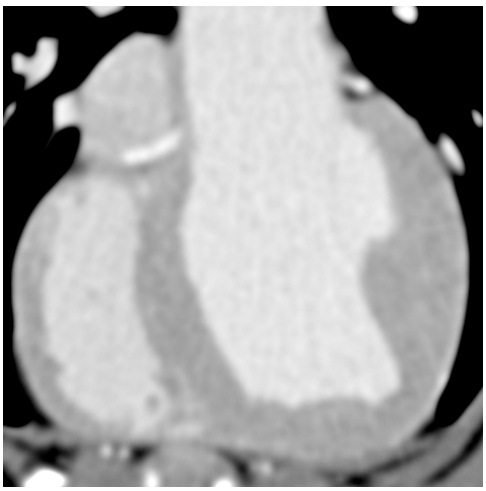

b) Score 1

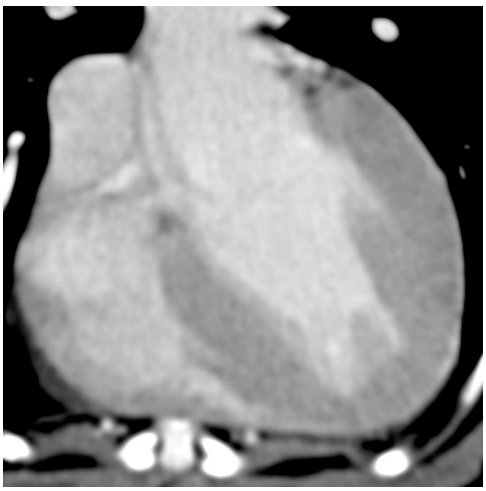

c) Score 0

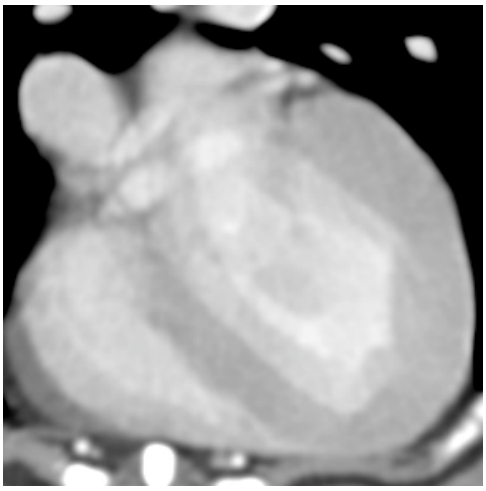

Figure 23. Transverse images at the level of the left ventricle

a) Score 2

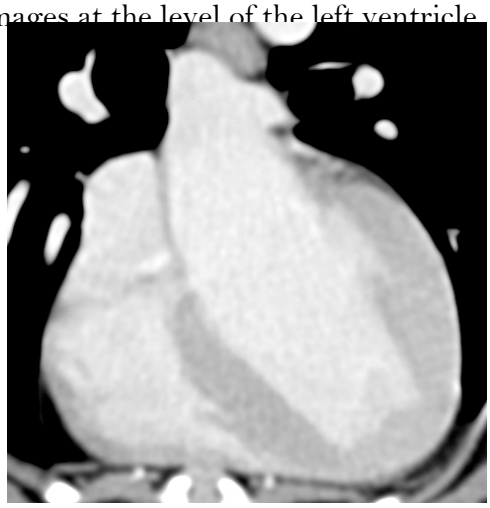

b) Score 1-N/A

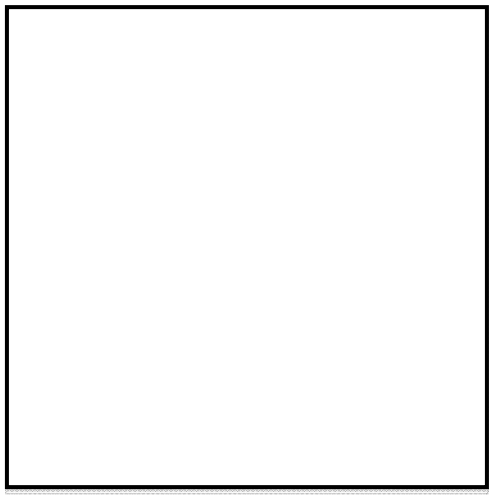

c) Score 0-N/A

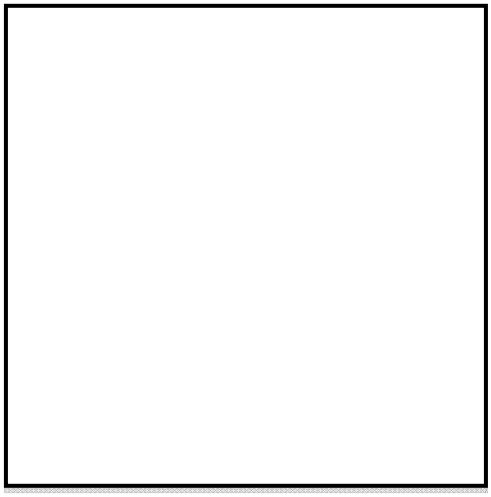

Figure 24. Transverse images at the level of the pulmonary veins.

Bibliography

1. Berrington de Gonzalez A, Mahesh M, Kim KP, et al. Projected cancer risks from computed tomographic scans performed in the United States in 2007. *Arch Intern Med* 2009;169:2071-2077.

2. Fox SH. Emerging developments in multidetector CT. Presented at the Advances in Multidetector CT Meeting 2003.

3. Bardo DM, Brown P. Cardiac multidetector computed tomography: basic physics of image acquisition and clinical applications. *Curr Cardiol Rev* 2008;4:231-243.

4. Computed Tomography (CT) Fastest Growing Medical Imaging Technology?: Marketstrat, Inc., 2010.

5. Weigold WG, Abbara S, Achenbach S, et al. Standardized medical terminology for cardiac computed tomography: a report of the Society of Cardiovascular Computed Tomography. *J Cardiovasc Comput Tomogr* 2011;5:136-144.

6. Drees R, Frydrychowicz A, Reeder SB, et al. 64-multidetector computed tomographic angiography of the canine coronary arteries. *Vet Radiol Ultrasound* 2011;52:507-515.

7. Ware WA. *Cardiovascular Disease in Small Animal Medicine*: Manson Publishing Ltd, 2007.

8. Evans HE, Miller ME. *Miller's anatomy of the dog*. 3rd ed. Philadelphia: W.B. Saunders, 1993.

9. Klaus-Dieter Budras PHM, Aaron Horowitz, Rolf Berg. *Anatomy of the Dog*. Fifth ed. Germany: Schlütersche Verlagsgesellschaft mbH & Co, 2007.

10. Moore RA. The coronary arteries of the dog. *American Heart Journal* 1930;5:743-749.

11. Buchanan JW. Pulmonic stenosis caused by single coronary artery in dogs: four cases (1965-1984). *J Am Vet Med Assoc* 1990;196:115-120.

12. Buchanan JW. Pathogenesis of single right coronary artery and pulmonic stenosis in English Bulldogs. *J Vet Intern Med* 2001;15:101-104.

13. Minami T, Wakao Y, Buchanan J, et al. A case of pulmonic stenosis with single coronary artery in a dog. *Nihon Juigaku Zasshi* 1989;51:453-456.

14. Kittleson M, Thomas W, Loyer C, et al. Single coronary artery (type R2A). *J Vet Intern Med* 1992;6:250-251.

15. Fonfara S, Martinez Pereira Y, Swift S, et al. Balloon valvuloplasty for treatment of pulmonic stenosis in English Bulldogs with an aberrant coronary artery. *J Vet Intern Med* 2010;24:354-359.

16. Tilley LP. *Manual of canine and feline cardiology*. 4th ed. St. Louis, MO: Saunders, an imprint of Elsevier Inc., 2007.

17. Sun JZ, Li ZY, Zang YM, et al. [Effect of beta-adrenergic agonist on segmental coronary arterial resistance in the dog]. *Sheng Li Xue Bao* 1987;39:296-299.

18. Tariq R, Kureshi SB, Siddiqui UT, et al. Congenital anomalies of coronary arteries: Diagnosis with 64 slice multidetector CT. *Eur J Radiol* 2011.

19. Sparrow P, Merchant N, Provost Y, et al. Cardiac MRI and CT features of inheritable and congenital conditions associated with sudden cardiac death. *Eur Radiol* 2009;19:259-270.

20. Chung JH, Gunn ML, Godwin JD, et al. Congenital thoracic cardiovascular anomalies presenting in adulthood: a pictorial review. *J Cardiovasc Comput Tomogr* 2009;3:S35-46.

21. Ou P, Marini D, Celermajer DS, et al. Non-invasive assessment of congenital pulmonary vein stenosis in children using cardiac-non-gated CT with 64-slice technology. *Eur J Radiol* 2009;70:595-599.

22. Bushberg JT. *The essential physics of medical imaging*. 2nd ed. Philadelphia: Lippincott Williams & Wilkins, 2002.

23. Lee JK, Sagel, S.S, Stanley, R. J. *Computed Body Tomography With MRI Correlation*. New York, New York: Raven Press, LTD, 1989.

24. *Cardiac imaging in electrophysiology*. New York: Springer, 2011.

25. *Cardiothoracic imaging with MDCT*. 1st ed. New York: Springer, 2008.

26. Rydberg J, Buckwalter KA, Caldemeyer KS, et al. Multisection CT: scanning techniques and clinical applications. *Radiographics* 2000;20:1787-1806.

27. Kopp AF, Schroeder S, Kuettner A, et al. Coronary arteries: retrospectively ECG-gated multi-detector row CT angiography with selective optimization of the image reconstruction window. *Radiology* 2001;221:683-688.

28. Rydberg J, Liang Y, Teague SD. Fundamentals of multichannel CT. *Radiol Clin North Am* 2003;41:465-474.

29. Mahesh M, Cody DD. Physics of cardiac imaging with multiple-row detector CT. *Radiographics* 2007;27:1495-1509.

30. Desjardins B, Kazerooni EA. ECG-gated cardiac CT. *AJR Am J Roentgenol* 2004;182:993-1010.

31. Ter-Pogossian MM, Weiss ES, Coleman RE, et al. Computed tomography of the heart. *AJR Am J Roentgenol* 1976;127:79-90.

32. Ter-Pogossian MM. Limitations of present radionuclide methods in the evaluation of myocardial ischemia and infarction. *Circulation* 1976;53:I119-121.

33. Skioldebrand CG, Ovenfors CO, Mavroudis C, et al. Assessment of ventricular wall thickness in vivo by computed transmission tomography. *Circulation* 1980;61:960-965.

34. Doherty PW, Lipton MJ, Berninger WH, et al. Detection and quantitation of myocardial infarction in vivo using transmission computed tomography. *Circulation* 1981;63:597-606.

35. Barter SJ, Steiner RE, Banks L, et al. Computed tomography of the heart: initial experience. *Clin Radiol* 1983;34:693-699.

36. Wood EH. New horizons for study of the cardiopulmonary and circulatory systems. *Chest* 1976;69:374-408.

37. McNitt-Gray MF. Tradeoffs in CT Image Quality and Dose.

38. Wilting JE. Technical Aspects of Spiral CT. *MedicaMundi* 1999;43:34-43.

39. Rémy-Jardin M. Rm, J. *Integrated Cardiothoracic Imaging with MDCT*. Verlag Berlin Heidelberg: Springer, 2009.

40. Lewis MA. Multislice CT: opportunities and challenges. *Br J Radiol* 2001;74:779-781.

41. Cody DD, Mahesh M. AAPM/RSNA physics tutorial for residents: Technologic advances in multidetector CT with a focus on cardiac imaging. *Radiographics* 2007;27:1829-1837.

42. Hong C, Becker CR, Huber A, et al. ECG-gated reconstructed multi-detector row CT coronary angiography: effect of varying trigger delay on image quality. *Radiology* 2001;220:712-717.

43. Raney AR, Saremi F, Kenchaiah S, et al. Multidetector computed tomography shows intramyocardial fat deposition. *J Cardiovasc Comput Tomogr* 2008;2:152-163.

44. Siripornpitak S, Pornkul R, Khowsathit P, et al. Cardiac CT angiography in children with congenital heart disease. *Eur J Radiol* 2011.

45. Rajiah P, Kanne JP. Computed tomography of septal defects. *J Cardiovasc Comput Tomogr* 2010;4:231-245.

46. Krauser DG, Cham MD, Tortolani AJ, et al. Clinical utility of delayed-contrast computed tomography for tissue characterization of cardiac thrombus. *J Cardiovasc Comput Tomogr* 2007;1:114-118.

47. Rajiah P, Kanne JP, Kalahasti V, et al. Computed tomography of cardiac and pericardiac masses. *J Cardiovasc Comput Tomogr* 2011;5:16-29.

48. Pannu HK, Jacobs JE, Lai S, et al. Coronary CT angiography with 64-MDCT: assessment of vessel visibility. *AJR Am J Roentgenol* 2006;187:119-126.

49. Giesler T, Baum U, Ropers D, et al. Noninvasive visualization of coronary arteries using contrast-enhanced multidetector CT: influence of heart rate on image quality and stenosis detection. *AJR Am J Roentgenol* 2002;179:911-916.

50. Guyton AC, Hall JE. *Textbook of medical physiology*. 11th ed. Philadelphia: Elsevier Saunders, 2006.

51. Scott AD, Keegan J, Firmin DN. Motion in cardiovascular MR imaging. *Radiology* 2009;250:331-351.

52. Pannu HK, Alvarez W, Jr., Fishman EK. Beta-blockers for cardiac CT: a primer for the radiologist. *AJR Am J Roentgenol* 2006;186:S341-345.

53. Ettinger SJ, Feldman EC. *Textbook of veterinary internal medicine : diseases of the dog and the cat*. 7th ed. St. Louis, Mo.: Elsevier Saunders, 2010.

54. Shim SS, Kim Y, Lim SM. Improvement of image quality with beta-blocker premedication on ECG-gated 16-MDCT coronary angiography. *AJR Am J Roentgenol* 2005;184:649-654.

55. Al-Kwifi O, Stainsby J, Foltz WD, et al. Characterizing coronary motion and its effect on MR coronary angiography--initial experience. *J Magn Reson Imaging* 2006;24:842-850.